國 立 交 通 大 學

電機與控制工程學系

博 士 論 文

利用虛擬實境場景誘發之暈車生理現象探討

Investigation of Physiological Responses Related to VR-induced Motion-Sickness

研 究 生： 陳 玉 潔
指導教授： 林 進 燈 教授

中 華 民 國 九 十 九 年 一 月

利用虛擬實境場景誘發之暈車生理現象探討

Investigation of Physiological Responses Related to VR-induced Motion-Sickness

研 究 生：陳玉潔　　Student：Yu-Chieh Chen

指導教授：林進燈 博士　　Advisor：Dr. Chin-Teng Lin

國立交通大學

電機與控制工程學系

博士論文

A Dissertation

Submitted to Department of Electrical and Control Engineering

College of Electrical Engineering

National Chiao Tung University

in partial Fulfillment of the Requirements

for the Degree of

Doctor of Philosophy

in

Electrical and Control Engineering

December 2009

Hsinchu, Taiwan, Republic of China

中 華 民 國 九 十 九 年 一 月

誌　　謝

在這學業即將完成之際，首先要感謝的是我的指導教授林進燈老師提供了豐富的研究資源和實驗環境，讓我們可以盡情的在知識的領域之中探索。除此之外，老師時常提醒我們要抓對重點，不偏離問題軸心，總是在大家茫然無措的時候為大家指出一條明路。在研究方面最要感謝的是 UCSD 的鍾子平老師與段正仁老師還有曲在雯博士，有您們不厭其煩的指導與建議，以及無數次的討論、檢討，才有現在的研究成果。在這段期間，我在您們身上學習到了做科學研究該有的態度，也學到了做事的方法，相信未來仍能受益良多。當然，這篇論文的完成，一定要感謝學弟尚文以及學妹君玲，與你們一起做研究的期間，讓我體會出團隊合作的可貴與重要性，更體會到了大家一起切磋、討論的愉快研究氣氛。沒有我們這個研究小隊，就沒有今天的研究成果可以發表，所以謝謝你們! 再來要感謝實驗室中小飛學長、學弟冠智、騰毅、欣泓、行偉、力碩、弘義、庭瑋、柏銓、嘉誠、青甫、華山以及學妹依伶，有你們的陪伴，研究生涯一點都不煩悶。

當然，最要感謝的就是我親愛的爸媽，感謝您們給我無憂無慮的生活環境，讓我長那麼大都不曾為了家計而擔憂。我知道，這是您們每日付出多大的辛勞，才換得到的。請您保重身體，不要讓自己太過操勞了!有您們無怨無悔的支持，永遠溫暖的懷抱，讓我可以勇敢的面對任何的挑戰。在博士修業的期間，我也曾經萌生退意，想快點進入職場工作；但因為您們的安慰與支持，讓我再次鼓起勇氣，決心將學業完成。因此，這份榮耀將永遠歸功於您們。

陳玉潔　敬上

2009/12/15

Abstract

This study investigates subjects' physiological responses related to motion-sickness using a virtual-reality-based driving simulator on a motion platform with six degrees of freedom, which provides both visual and vestibular stimulations to induce motion-sickness in a manner that is close to that in daily life. The degree of motion-sickness was simultaneously and continuously reported by the subjects using an onsite joystick, providing non-stop behavioral references to the recorded biomedical signals. This study assesses the temporal relationship between heart rate variability (HRV) and the level of motion sickness (MS). Compared to the baseline (low MS) session, the low-frequency (LF, 0.04–0.15Hz) and the ratio of low- to high-frequency (LF/HF) components of HRVs increased significantly, while the HF (0.15–0.4Hz) component decreased when the self-report MS level increased. This finding is consistent with a perception-driven autonomic response of the cardiovascular system. Moreover, adaptive neural fuzzy inference system (ANFIS) was used to assess and model the relation between the HRV indices and MS severity. The results of this study showed that a combination of LF and HF indices and their ratio was strongly correlated with changes of the subjective ratings of MS, suggesting that MS may affect the combination of the sympathovagal interactions. Subjects' brain dynamics associated with motion sickness were measured using a 32-channel EEG system. The acquired EEG signals were parsed by independent component analysis (ICA) into maximally independent processes. The decomposition enables the brain dynamics that are induced by the motion of the platform and motion-sickness to be disassociated. Five MS-related brain processes with equivalent dipoles located in the left motor, the parietal, the right motor, the occipital and the occipital midline areas were consistently identified across the subjects. The parietal and motor components exhibited significant alpha power suppression in response to vestibular stimuli, while the occipital components exhibited MS-related power augmentation in mainly theta and delta bands; the occipital midline components exhibited a broadband power increase. Further, time series cross-correlation analysis was employed to evaluate relationships between the spectral changes associated with different brain processes and the degree of motion-sickness. According to our results, it is suggested both visual and vestibular stimulations should be used to induce motion-sickness in brain dynamic studies.

Contents

1 Introduction

1.1 What is Motion-sickness

Motion-sickness (MS) is a common experience of numerous people. The symptoms of MS are headache, eye strain, pallor, sweating, disorientation, postural instability, vertigo, nausea, and vomiting. The symptoms of motion-sickness are not identical to everyone. About 33% of people are susceptible to motion sickness even in mild circumstances such as being on a boat in calm water, and nearly 66% of people are susceptible in more severe conditions. Turner and Griffin (1999) performed a questionnaire survey to identify personal and environmental factors influencing individual susceptibility to motion sickness during road transport in passengers. Overall, 28.4% of passengers reported feeling ill, 12.8% reported nausea and 1.7% reported vomiting during travel. Kellog et al. (1980) described that the malaise of sickness may last for more than one hour, and Gower et al. (1989) further proved that the duration of sickness can even last for one day. Many previous studies have indicated that the malaise of sickness can sometimes cause self-control ability decline and lead to serious traffic accident fatalities. Thus there have been numerous attempts made by scholars to understand motion sickness and the caused symptoms.

1.2 Theories of Motion-sickness

There are several theories behind the concept of motion-sickness. The three most popular theories will be presented in this research, including sensory conflict theory, poison theory and postural instability theory. The three theories explain three different status of motion-sickness. For example, the sensory conflict theory gives a general concept of motion-sickness induction; the postural instability theory explains how men react to motion-sickness and the poison theory explains syndrome (i.e. vomiting) of motion-sickness.

1.2.1 Sensory Conflict Theory

The sensory conflict theory (Reason & Brand, 1975) that came about in the 1970's has become the most accepted explanation of motion-sickness. The theory indicated that the conflict between the incoming information could induce motion-sickness. The vestibular system, shown in Fig. 1-1, provides information about the movement and orientation of the head in space. It is comprised of the non-acoustic portion of the inner ear which consists of three semicircular canals for detecting angular acceleration and the utricle and saccule which detect linear acceleration.

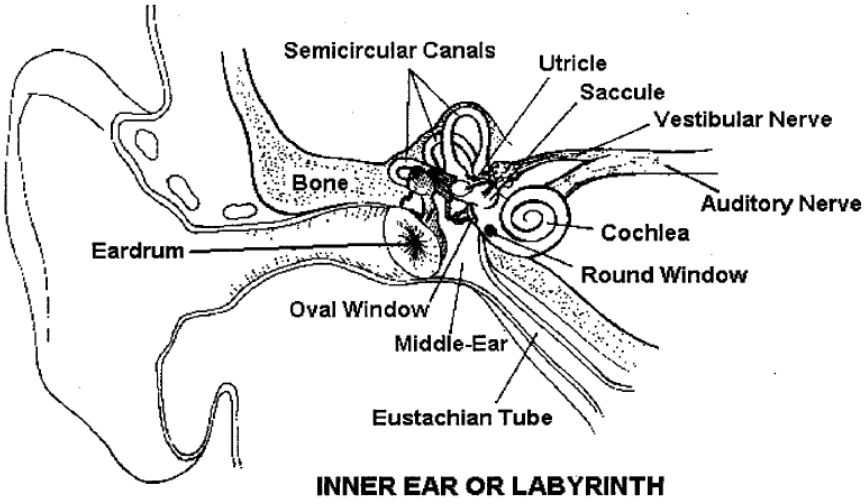

Fig. 1-1. The vestibular system in the inner ear.

The three semicircular canals correspond to each of the three dimensions in which human movement. Each canal is filled with a fluid called endolymph, which flows through the canal as the head experiences angular acceleration. As the fluid flows through the canal (as shown in Fig. 1-2), it deflects small hair-like cells, called cupula, which send signals to the vestibular receiving areas of the brain.

There are two vestibular components, one on each side of the head, acting in a push-pull manner. Since each group of hair cells is polarized, they can be either excited (pushed) or inhibited (pulled) based on which direction the cupula move. It is important for both vestibular apparatuses to agree with each other. One side should push and the other should pull in normal conditions, and vertigo will result if both sides are pushed (or pulled).

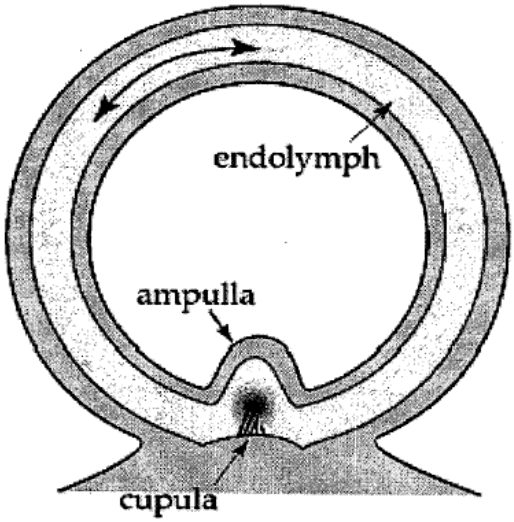

Fig. 1-2. A cross section of a semicircular canal. The cupula sit in a small swelling at the base of the canal called the ampula.

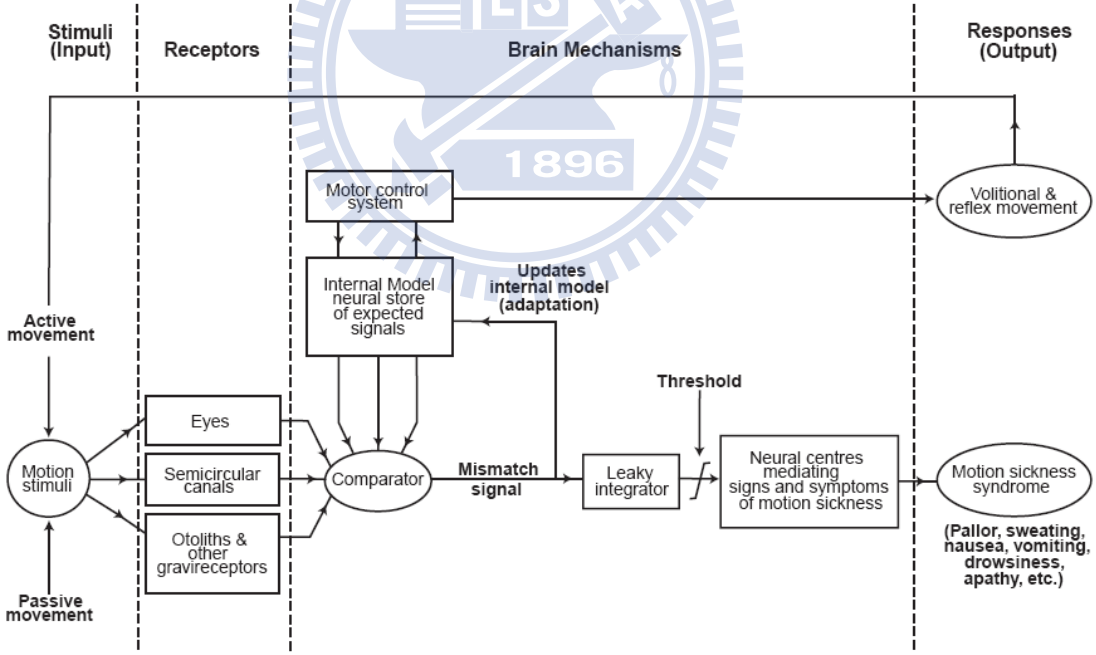

Fig. 1-3. A heuristic model of motor control, motion detection, and motion sickness based on the sensory conflict theory. (Benson, 1984)

The principal concepts of the sensory conflict theory are shown in Fig. 1-3. Essential to the theory is the presence within the brain of a representation of afferent and efferent activity associated with bodily movement. This internal model is built up from information acquired during normal locomotor activity and the control of balance and posture. Combinations of motion stimuli, including active and passive movements, are sent to receptors as input information of the model. Input information about bodily orientation and movement comes from sensory organs stimulated by bodily motion, such as the eyes, the semicircular canals and otolith organs and mechanoreceptors in the skin, capsules of joints, and muscles. A comparator in brain compares the information from the internal model and the receptors and calculates the mismatch signals for updating the model.

Furthermore, vestibular information plays important roles in perceptual tasks such as ego motion estimation. More recently, vestibular information was shown to disambiguate the interpretation of dynamic visual information experienced simultaneously during observer's movement. As an example, considering the constant small wavers and rocking back and forth when someone is trying to stand still. This is a direct reflection of the vestibular system at work.

Under normal circumstances, the brain gathers information using the eyes, the inner ear, expectations and previous experiences. The problem begins when the brain

receives visual and sensory clues that contradict each other. For example, if someone is inside a ship, with no view of the horizon, the room appears to be still but the balance mechanism in his inner ear detects that he is rocking back and forth when motion sickness begins.

1.2.2 Poison Theory

The sensory conflict theory permits the identification of different kind of mismatch signals. However, it does not explain why humans respond by vomiting. Emesis is clearly of benefit to an animal as a means of getting rid of ingested poison. Treisman (1977) postulated that brainstem mechanisms subserving orientation and motion also detect neurophysiological dysfunction caused by a neurotoxin and initiate the teleologically beneficial response of vomiting. He further hypothesized that in motion-sickness, vomiting occurs because this protective mechanism interprets conflicting sensory signals as neural dysfunction caused by poisoning.

1.2.3 Postural Instability Theory

The postural instability theory (Riccio & Stoffregen, 1991) is centered on the idea of maintaining postural stability in the environment. For example, consider walking on concrete and walking on ice. The natural reaction to walking on ice is to change the walking pattern to maintain postural stability. Whenever the environment changes

in an abrupt or significant way, in many cases, postural control will be lost especially if the control strategies are not available due to lack of experience. Eventually, the control strategy will be learned and postural stability will be attained once again. When someone has either degraded or completely lost postural control, they are in a state of postural instability. The theory perfectly explains why people can “learn” to get used to a VR scene and they won’t feel sick if they practice enough.

1.3 Modalities to Induce Motion-sickness

According to sensory conflict theory, motion sickness (MS) is considered a consequence of conflicts in perceptions originated from the visual, vestibular and proprioceptive systems (Redfern *et al*., 2001; Klosterhalfen *et al*., 2000; Drummond, 2002). Experimental MS is commonly induced in virtual reality (VR) environments (Riva, 1998; Lin *et al*., 2002) or by a rotating drum with or without optokinetic stimulation (Drummond, 2002; Wan *et al*., 2003). However, it is unclear whether VR-induced or rotating-drum-induced MS involves the same underlying neural mechanisms as that in daily life experiences such as automobile driving (Golding, 2006). According to sensory conflict theory, we understand that induction of motion-sickness is take place in brain with the signals transferred from plenty of sensors in our body. Thus it is suggested to conduct a motion-sickness experiment

with applying similar conditions to the real situation. However, most of the MS experiments involved a single modality using either visual (Hu *et al.*, 1999; Kim *et al.*, 2005; Lo & So, 2001; Min *et al.*, 2004) or vestibular inputs (Wood *et al.*, 1991; Wood *et al.*, 1994; Wu, 1992; Chelen *et al.*, 1993). This single-modality scheme may be unrealistic and suboptimal for reliably inducing motion-sickness in subjects and, leading to inconsistent results concerning changes in EEG power.

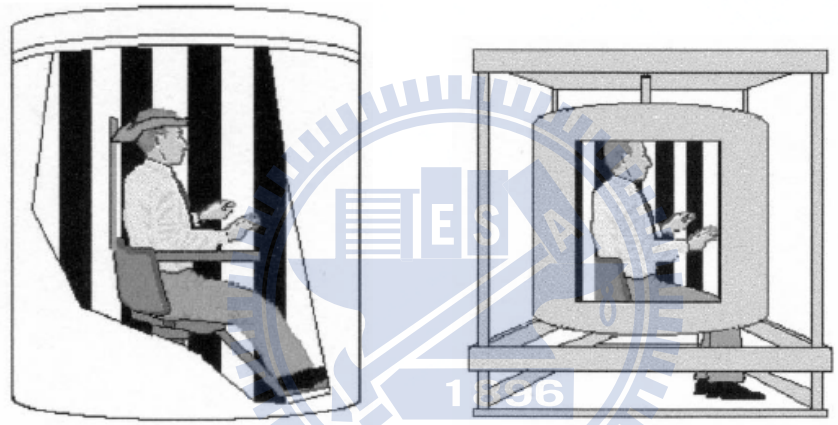

Fig. 1-4. Traditional methods used by scholars to induce motion-sickness: (A) A rotating chair in a metal cylinder, (B) a rotating drum in a metal cylinder.

Vestibular stimuli were normally provided to the subjects with rotating chair (Wood et al., 1991; Wood et al., 1994), parallel swing (Wu, 1992), and cross-coupled angular stimulation (Chelen et al., 1993) to induce motion-sickness. Theta power increases in frontal and central area were reported in a parallel swing study (Wu, 1992). Significant increase in theta wave activity in the frontal areas was presented in a motion-sickness study by using rotating drum (Wood et al., 1991; Wood et al., 1994).

Chelen et al. (1993) employed cross-coupled angular stimulation to induce motion-sickness symptoms and found mean power spectral energy in the delta and theta band during sickness increased while mean alpha band energy was not significantly different.

Visually induced motion-sickness is also very popular among the previous studies. The typical case of visually induced sickness can be provoked with an optokinetic drum rotating vertically about a stationary subject's yaw axis. This situation can cause a compelling sense of self-motion (called vection). Vestibular cues indicate that the body is stationary, whereas visual cues report the body is moving. Hu et al. performed an experiment by using optokinetic rotating drum to study motion-sickness and found a higher net percent increase of spectral power in EEG frequency band 0.5-4 Hz between drum rotation and baseline periods on C3 and C4 (Hu et al., 1999). Besides, compelling scene movements in a virtual reality (VR) system can also cause symptoms of motion-sickness (Lo & So, 2001) (i.e., cybersickness). Delta power increases in frontal and temporal area were reported in an object-finding VR experiment (Kim et al., 2005), accompany with beta power decrease in same brain areas. Delta power increases were also reported in a car-driving VR experiment performed by Min et al. (2004). However, they also found the theta power decreases were highly correlated with sickness level.

1.4 Assessment of Motion-Sickness

Another important factor in motion-sickness experiments has been the degree of sickness of the participants. Many scholars have adopted a motion-sickness questionnaire by Kennedy *et al.*, (1993) to measure susceptibility of subjects to MS. It is a standard rating system for comparing MS states among subjects. However, it demands interrupting the experiments and asking the subjects to answer few questions. This approach may not be practical for a continuous performance task, in which subjects must perform the task continuously. For example, in a long-term driving experiment in which the subject's cognitive states are monitored, interrupting the experiment for the questionnaire may arouse the subjects. Moreover, such intervention may influence human physiology which makes it very difficult or even possible to correlate the measured physiological signals with the motion-sickness level. Therefore, an easy-to-operate online rating mechanism is sought to record continuously the level of motion-sickness in subjects.

The focus of early motion-sickness studies was on the physiological changes related to motion-sickness. For instance, the electrogrstrography (EGG) signals (Hu et al., 1991; Cheung & Vaitkus, 1998) have been employed to detect symptoms of motion-sickness, such as vomiting, and galvanic skin responses (GSR) have been used to detect sweating. Holmes & Griffin (2001) observed increased heart rate

variability (HRV) during nausea, indicating the modulation of the automatic nervous system (ANS) in motion-sickness. Rapid advances in neuroimaging technology have enabled the neural correlates of motion-sickness to be examined. Electroencephalography (EEG) is one of the best methods for monitoring the brain dynamics induced by motion-sickness because of its high temporal resolution and portability.

1.4.1 Previous EEG Studies

Wu (1992) showed that theta power increases in the frontal and central areas when subjects were placed in a moving parallel swing device. Wood *et al.* (1991, 1994) also found increased EEG theta wave in the frontal areas during motion-sickness induced by a rotating drum. Chelen *et al.* (1993) adopted cross-coupled angular stimulation to induce motion-sickness and found increased delta- and theta-band power during sickness but no significant change in alpha power. Hu *et al.* (1999) investigated MS triggered by the viewing of an optokinetic rotating drum and found a higher net percentage increase in EEG power in the 0.5-4 Hz band at electrode sites C3 and C4 than in the baseline spectra. Kim *et al.* (2005) found increases in both delta and beta power in the frontal and temporal areas in an object-finding VR experiment. Min *et al.* (2004) also found increases in delta power in a car-driving VR experiment. However,

they also found that theta power declined as the degree of motion-sickness increased.

Motion-sickness-induced EEG power changes are not consistent among all of the cited studies. One reason may be the wide range of paradigms used to induce motion-sickness. Most of the above-mentioned experiments involved a single modality using either visual (Hu *et al.*, 1999; Kim *et al.*, 2005; Lo & So, 2001; Min *et al.*, 2004) or vestibular inputs (Wood *et al.*, 1991; Wood *et al.*, 1994; Wu, 1992; Chelen *et al.*, 1993). This single-modality scheme may be unrealistic and suboptimal for reliably inducing motion-sickness in subjects and, leading to inconsistent results concerning changes in EEG power.

1.4.2 Previous HRV Studies

The MS symptoms are associated with perturbed sympathovagal activities (Xu *et al.*, 1993; Jang *et al.*, 2002; Gianaros *et al.*, 2003). Specifically, heart rate (HR) increases in response to exposure to nauseogenic bodily motions (Cowing *et al.*, 1986 and 1990) or to optokinetic stimulation (Hu *et al.*, 1991; Uijtdehaage *et al.*, 1993). Power spectral analysis of electrocardiographic (ECG) (R–R) intervals is considered a reliable and sensitive measurement of MS-induced sympathovagal perturbation in humans (Stys & Stys, 1998). For instance, MS severity changes linearly with changes in the power spectral density (PSD) of the R-R interval time series (Doweck *et al.*,

1997). The following three spectral components are identified in the spectrum of R-R interval time series (Kuo *et al*., 1999; Bolanos *et al*., 2006): very low frequency (VLF) (0.003 – 0.04 Hz), low frequency (LF) (0.04 – 0.15 Hz) and high frequency (HF) (0.15 – 0.4 Hz) components. The power distribution and center frequency of LF and HF components reflect the autonomic neural modulations of heartbeats. The LF component of HRV is mediated by both sympathetic and parasympathetic activities (Goichot *et al*., 2004; Chen *et al*., 2005; Casu *et al*., 2005) and the parasympathetic activity is recognized as a major contributor to the HF component (Beckers et al., 2006; Stauss, 2003; Emoto et al., 2007).

The underlying physiological mechanism of the VLF component remains unclear and its reliability is controversial (Camm *et al*., 1996; Kato *et al*., 2004; Pipraiya *et al*., 2005). The LF/HF ratio is typically considered to reflect sympathetic/parasympathetic balance at cardiac rhythms (Franchi *et al*., 2001; Wodey *et al*., 2003; Demaree & Everhart, 2004). Previous studies that examined the relationship between the degree of MS and the automatic nervous system (ANS) typically compared averaged heart rate variability (HRV) indices before and during experimental motion exposure over a period (e.g., Hu *et al*., 1991; Uijtdehaage *et al*., 1993). Therefore, short-term or transient pattern of autonomic control of HRV may obscure important information (Morrow *et al*., 2000). Only one study correlated MS with temporal changes in HRV

(Gianaros *et al*., 2003) and demonstrated that HF power decreased as MS severity increased. In previous studies, the severity of induced MS was assessed subjectively and intermittently. For example, MS symptoms were verbally reported at 1-min intervals (Holmes & Griffin, 2001; Young, 2003; Ziavra *et al*., 2003). Such intervention can unexpectedly introduce room for subjects to temporally reduce their MS to an undetermined extent and adversely influence the interrelationship between MS and HRV estimates (Forstberg *et al*., 1998; Sang *et al*., 2003). Studies using a high temporal resolution and with minimal measurement interventions are required to accurately correlate HRV indices with MS severity.

1.5 The Proposed Research

This study demonstrates a VR-based motion-sickness platform that comprises a 32-channel EEG and 2-channel ECG system, and a joystick with a continuous scale, where by subjects can continuously report their level of motion-sickness during experiments. All measurements, including the level of motion-sickness and the motion of the platform, were synchronized with EEG and ECG recordings. The VR-based platform simultaneously provides both visual and vestibular stimuli to generate a most realistic experimental environment for studying motion-sickness.

This study first attempted to correlate the HRV indices with the MS severity; both

were recorded continuously using an ECG and a slide-type switch during a simulated driving experiment. Experiments were conducted on a motion driving simulator comprising a VR-based tunnel driving environment and a real vehicle mounted on a 6 degree-of-freedom motion platform (Lin *et al*., 2005a; 2005b). The temporal correlation between changes in the MS severity and the HRV indices was assessed and modeled by non-linear regressive algorithms — adaptive neural fuzzy inference system (ANFIS). Some subjects who had autonomic responses opposite to those of the majority of subjects during MS exposure. These subjects (n=6 among a total of 29 subjects) likely failed to respond to VR stimulation. These subjects reported that they felt sickness immediately after the onset of the experiment. Such early onset sickness could be induced by the unfamiliar with the VR-scene. The subjects were further excluded from EEG data analysis.

The recorded EEG signals are analyzed using independent component analysis (ICA), time-frequency analysis, and time-series cross-correlation to investigate MS-related brain dynamics in a continuous driving task. Independent EEG activities and their equivalent dipole source locations were isolated by independent component analysis (ICA) to obtain the involved brain circuits during motion-sickness. The ICA signals were then correlated to the MS level to investigate the changes before, during and after motion-sickness induce session. The temporal relationship between the

reported sickness-level and the involved brain circuits were then determined by cross-correlation analysis.

2 Material and Methods

Unlike previous studies, we facilitated both visual and vestibular stimuli to the subjects in a realistic environment that comprises a 360^{o} projection of VR scene and motion platform with six degrees of freedom (DOF) to induce motion-sickness. It is expected to induce motion-sickness in a manner consistent with real-life experience. During the experiments, the subjects were asked to sit inside a model car that was mounted on the motion platform as passengers, with their hands on a joystick that was used to continuously report their sickness level.

2.1 Experimental Protocol

Fig. 2-1 The virtual-reality environment.

For the reason of safety and reality, the virtual reality (VR) technology is used in our experiments to induce motion sickness. It takes the advantages of low cost, reality and time saving. The VR scene combined with the Stewart dynamic platform can provide the visual and kinesthetic stimuli to subjects, as shown in Fig. 2-1.

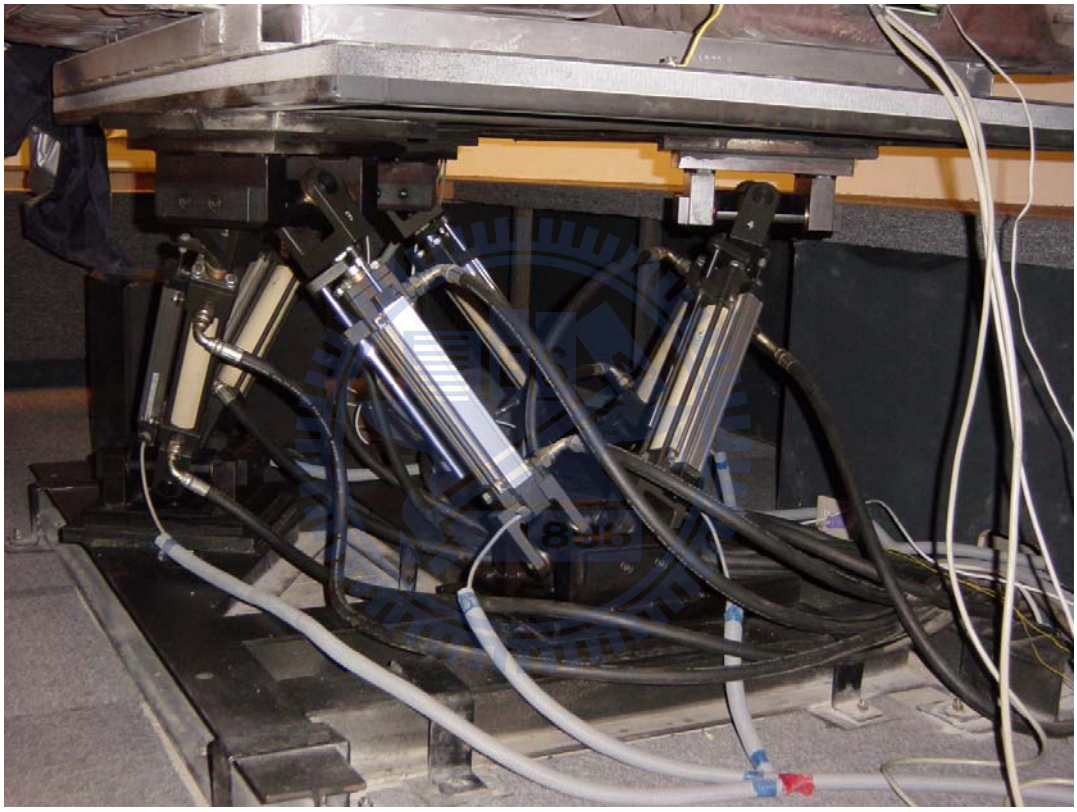

Fig. 2-2. The Stewart platform in NCTU Brain Research Center.

A typical Stewart platform has a lower base platform and an upper payload platform connected by six extensible legs with ball joints at both ends as shown in Fig. 2-2. A Stewart platform is also called a six-degree-of-freedom motion platform, which

means the payload platform of the system has 6-dimension of freedom, including the X, Y, and Z translational movements, and the Roll, Pitch and Yaw rotational movements. Positions of the payload platform in the applications can be decided according to the six parameters.

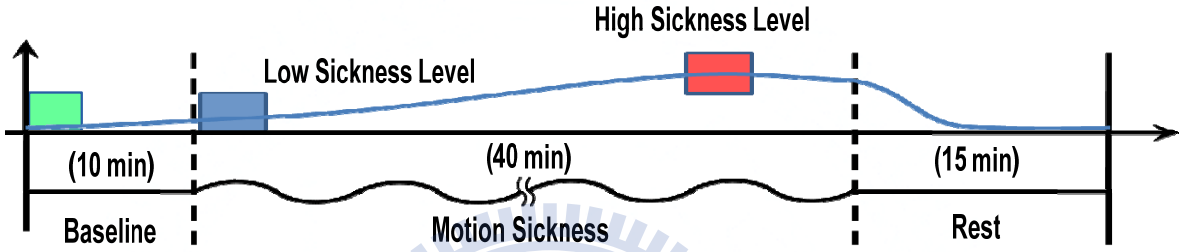

Fig. 2-3. Experimental design of the motion-sickness research.

The subjects can interact directly with the environment and perceive more realistic driving conditions during the experiments. An auto-driving VR scene in a tunnel was programmed to eliminate any possible visual distraction and shorten the depth of the visual field such that motion-sickness could be easily induced. A three-section experimental protocol (Fig. 2-3) was designed to induce motion-sickness. First, the baseline section involved 10 minutes of driving on a straight road to record the subjects' baseline EEG. Then, a winding road was presented to the subjects for 40 minutes to induce motion-sickness. Finally, a recovery section that involved cruising

on a straight road was presented for 15 minutes to help the subjects to recover from the sickness. The level of sickness was continuously reported by the subjects, using a joystick with a continuous scale on its side. The experimental setting successfully induced motion-sickness in more than 80% of the subjects herein this investigation.

2.2 Signal acquisition

Thirty two-channel EEG signals were acquired at a sampling rate of 500 Hz using a NuAmps (BioLink Ltd., Australia). The electrode locations were based on a standard thirty two-channel system provided in a freely downloadable Matlab toolbox, EEGLAB (http://sccn.ucsd.edu/eeglab). The acquired EEG signals were first inspected to remove bad EEG channels, and then down-sampled to 250 Hz. A high pass filter with a cut-off frequency at 1 Hz with a transition band of 0.2 Hz was used to remove baseline-drifting artifacts. Then, a low pass filter with a cut-off frequency of 50 Hz and a transition band of 7 Hz was applied to the signal to remove muscular artifacts and line noise. Photos of the NuAmps amplifier and the electrode cap are shown in Fig. 2-4. The 10-20 International System of Electrode Placement standard to place the EEG electrodes (Jasper, 1958), was used in this study. An illustration of the 10-20 system is shown in Fig. 2-5.

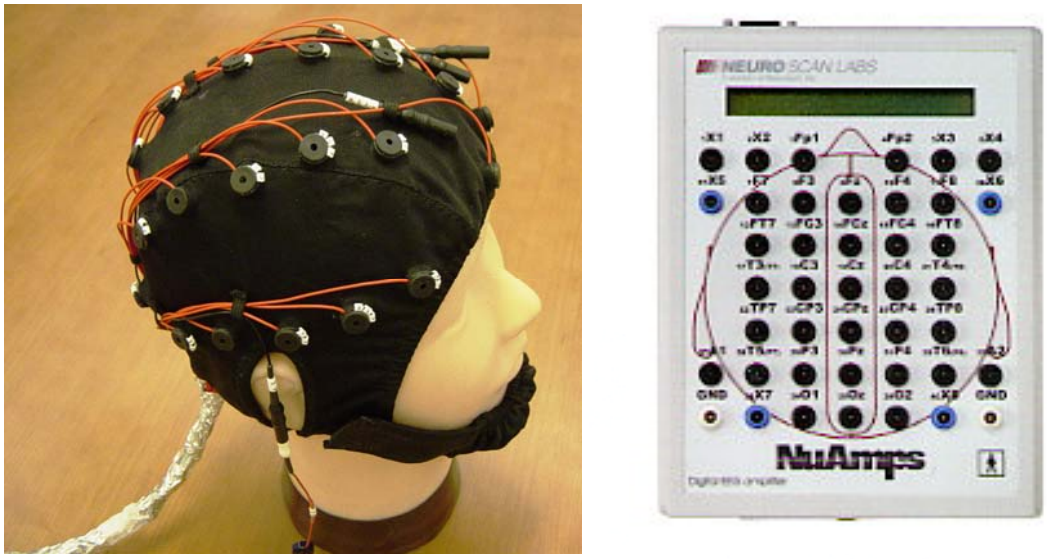

Fig. 2-4. The electrode cap and the EEG signal amplifier.

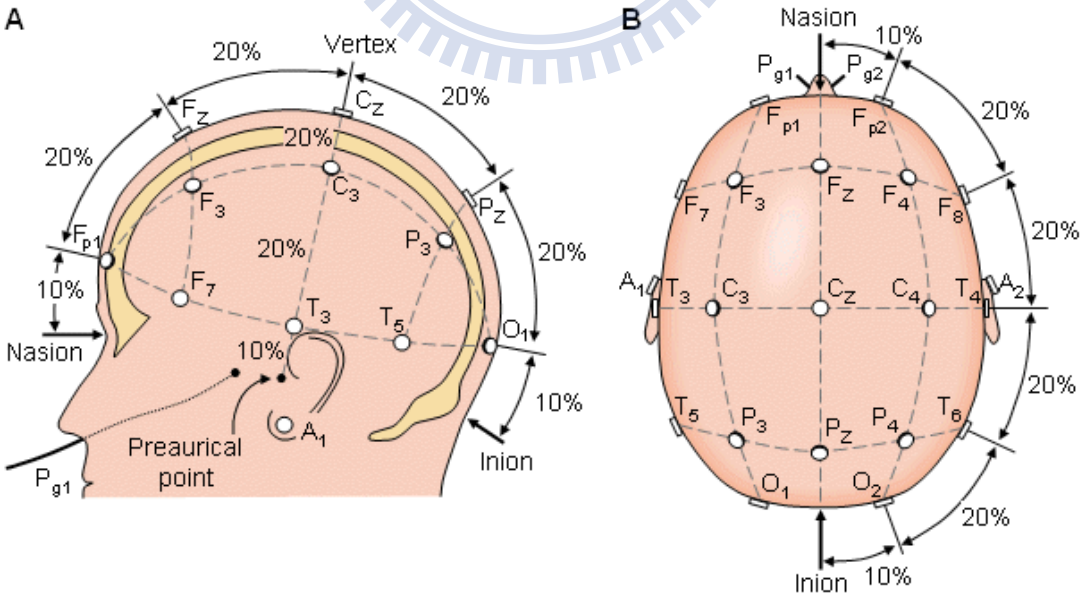

Fig. 2-5. The 10-20 international electrode placement system.

The level of sickness was continuously reported by each subject using a joystick with a continuous scale, which was synchronized to the EEG signals. The subjects were told to push the joystick to a higher level if they felt more sick comparing to the last condition. The sickness level ranged from zero to five. Such continuous sickness level was reported in real-time without interrupting the experiment, in contrast with the traditional motion-sickness questionnaire (MSQ). After finishing the experiment, each subject was required to fill a MS questionnaire (modified from Holmes & Griffin, 2001; Yokota *et al*., 2005) to recall the levels of MS during the experiment, and report what kind of behavioral adjustment they used when they feel uncomfortable. In the questionnaire, the subjects used 6 levels (0 – 5) to report their symptoms of MS (with 0 = no MS, 1 = stomach awareness, 2 = stomach discomfort, 3 = slight nausea, 4 = moderate, and 5 = severe nausea). In the main experiment, subjects' ECG data were also recorded for evaluating the relationship between HRV indices and MS severity. Electrocardiogram signals were acquired by two electrodes in a modified leads II configuration (Griffiths, 2007). The positive and negative leads were placed on the left arcus costalis and right clavicle, respectively. The ECG signals were amplified (NuAmps, Compumedics Ltd., VIC, Australia) and recorded at a sampling rate of 500 Hz, and notch filtered at 60 Hz. The ECG signals and MS severity were synchronized to trigger signals generated by the MS rating device.

2.3 Subjects

A total of 29 volunteers (15 females and 14 males; mean age, 23 ± 2 years) with normal or corrected-to-normal vision were paid to participate in this MS experiment. All subjects were healthy and had no history of gastrointestinal, cardiovascular, neurological and psychological disorders. Subjects were required not imbibe alcoholic or caffeinated drinks, or to participate in strenuous exercise 1 day prior to the experiments. The experiments were performed in the morning (9 – 12 AM) or afternoon (2 – 5 PM). Subjects were required to fast for 2 hrs prior to the experiments. Experiment protocol was approved by the Institutional Review Broad of Taipei Veterans General Hospital, Taiwan. Subjects were informed of the experimental procedure and written consent was obtained from each subject prior to the experiment. Some subjects who had autonomic responses opposite to those of the majority of subjects during MS exposure. These subjects (n=6 among a total of 29 subjects) likely failed to respond to VR stimulation. These subjects reported that they felt sickness immediately after the onset of the experiment. Such early onset sickness could be induced by the unfamiliar with the VR-scene. The subjects were further excluded from EEG data analysis. Furthermore, four subjects were excluded from EEG analysis due to the EEG signals quality.

2.4 Data Analysis

2.4.1 Analysis of EEG Signals

ICA and IC clusters

The filtered EEG signals were first decomposed into independent brain sources by independent component analysis (ICA) (Bell & Sejnowski, 1995; Makeig *et al.*, 1997) using EEGLAB (Delorme & Makeig, 2004). The ICA algorithm can separate N source components from N channels of EEG signals. The summation of the EEG signals at the sensors is assumed to be linear and instantaneous, i.e. the propagation delays are negligible. We also assume that the time courses of muscle activity, eye, and, cardiac signals are not time locked to the EEG activities reflecting synaptic activity of cortical neurons. Therefore, the time courses of the sources are assumed to be statistically independent. The multi-channel EEG recordings are considered as mixtures of underlying brain sources and artifacts. The source signals contribute to the scalp EEG signals through a fixed spatial filter. Such a spatial filter can be reflected by the rows of inverse of unmixing matrix, W in u = Wx, where u is the source matrix and x is the scalp-recorded EEG. The spatial filters can be plotted as the scalp topography of independent component. The scalp topography of each independent component (IC) can be further analyzed using DIPFIT2 routines (Oostendorp & Oostenveld, 2002), a plug-in in EEGLAB, to find the 3D location of

an equivalent dipole or dipoles based on a four-shell spherical head model. Then, components with similar scalp topographies, dipole locations and power spectra from many subjects were further grouped into component clusters to examine the consistency of brain areas involved in the task. Ten component clusters recruited more than 10 components from multiple subjects with similar topographic maps. Among these robust component clusters, we further correlated the component power spectra with subjects' continuous motion-sickness rating. Average correlation coefficient was computed for each of the robust component clusters. Then, the five most motion sickness level-related clusters were selected for further analysis.

Relationship between spectra and road-condition or motion-sickness

As mentioned above, brain signals can be sensitive to any environmental change. Hence the EEG signals acquired under various conditions (such as on a straight or curved road) should not be confounded by motion-related activities. For example, when the experiment entered the winding-road riding section, the car began to sway left and right with the VR scene of the curved road, providing both visual and body sensation stimuli to the subjects. This baseline difference among EEG power spectra associated with the different road conditions must be considered when the MS-related EEG power changes are evaluated.

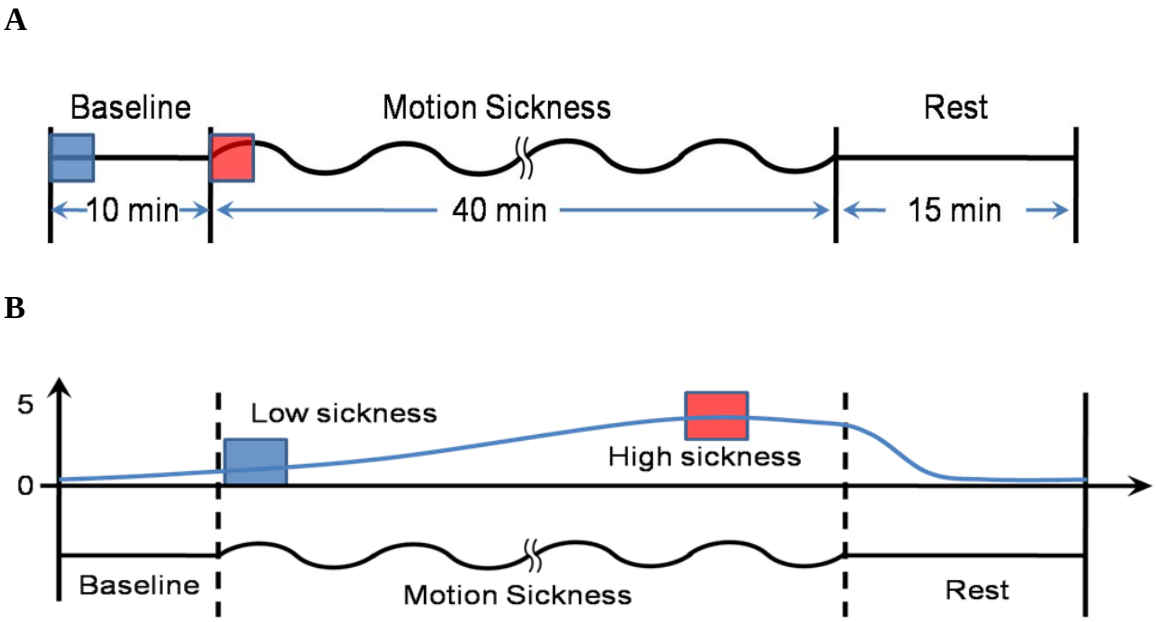

Fig. 2-6. Road-condition and motion-sickness effects can be extracted from the signals by comparing EEG signals in the red and blue blocks.

Therefore, the EEG power spectral changes in three periods were initially examined: (1) baseline - the first 200 seconds of the baseline straight road section, (2) low MS level - the first 200 seconds of the curved road section, and (3) high MS level - the first 200 seconds after the highest sickness rating (Fig. 2-6 B). The power spectra in these three time periods (baseline, low-sickness and high-sickness) were then averaged among subjects in each selected IC cluster.

A statistical analysis was also conducted to assess the significance of the spectral differences of the independent components under different motion-sickness levels and various road conditions. Since the true sample distribution of the component spectra

was unknown and the sample size (n=19 as 5 of 23 subjects were excluded due to low quality of EEG data) was small, a nonparametric statistical analysis, a paired-sample Wilcoxon signed-rank test, was employed to access the statistically significant spectral differences between different conditions. The level of significance was set to $p < 0.01$.

Time-frequency Analysis

Time-frequency analysis was utilized to test the dynamics of the ICA power spectra throughout the experiment. The time series of the ICA power spectra were then correlated with the continuous sickness-level to determine the MS-related spectral changes. The frequency responses of ICA activations were calculated using a 500-point moving window with 250 overlapping points. The 500-point epochs were further subdivided into several 125-point sub-windows with 25-point overlaps. The 125-point sub-windows were zero-padded to 512 points to calculate the power spectra using a 512-point fast Fourier transform (FFT), yielding an estimate of the power-spectrum density with a frequency resolution of 0.5 Hz. The power spectra of these sub-windows were then averaged to produce a power spectrum for each 2 s epoch. The power spectrum density (PSD) was then converted into dB power. The temporal resolution of the resultant spectral time series was 1 s since the window step

was 250 points and the EEG was sampled at 250 Hz. The analysis procedure is shown in Fig. 2-7.

It is possible that both road condition (i.e., the big sway of the VR driving model) and motion-sickness level can simultaneously alter EEG power spectrum. Here, a two-stage baseline removal was used to dissociate the baseline EEG power spectrum associated with different road conditions. First, we computed the baseline EEG power of the baseline section by averaging the first 3-minute EEG power spectrum of the baseline section and subtracted this baseline EEG power from the entire EEG signal. Second, we computed the baseline EEG power from the first 3 minutes of EEG signals acquired during the motion-sickness section and subtracted this baseline EEG power only from the EEG signals of the motion-sickness section. We assumed that the EEG power changes caused by the moving platform would be consistent through the entire motion-sickness section and, thus, we could extract mainly the motion-sickness related EEG power changes by removing the baseline EEG power derived from the beginning of this section. However, there might be interaction between the level of movement of the platform and motion-sickness level. This remains a question for further exploration. In this study, we tried to program the movement of platform as consistent as possible through the motion-sickness section and kept this parameter well controlled.

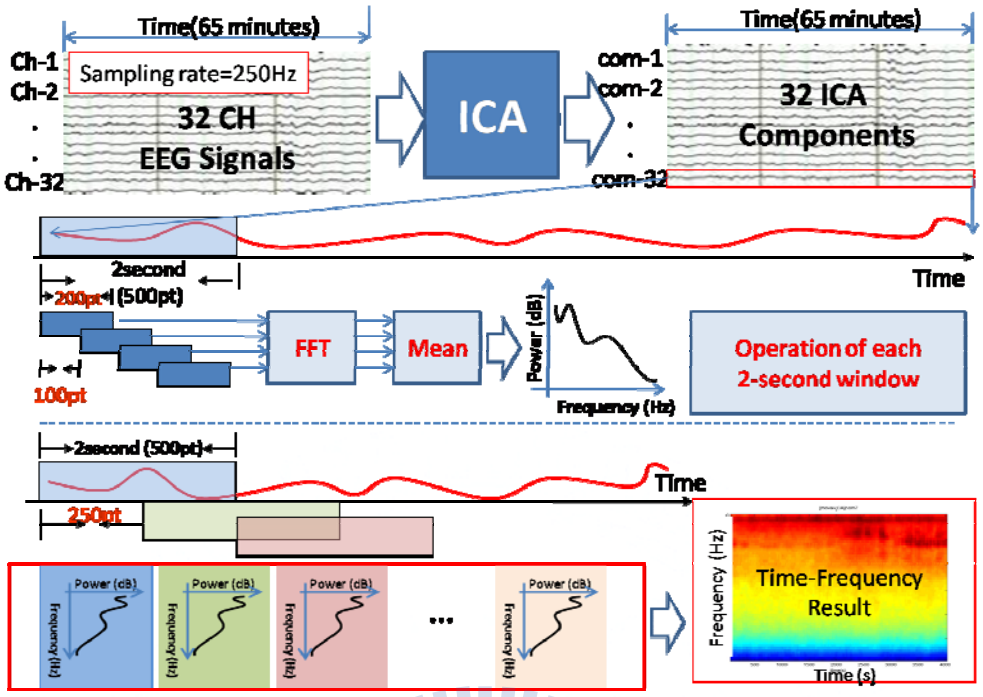

Fig. 2-7. Time-frequency analysis procedure used to obtain dynamic EEG frequency responses during the experiments.

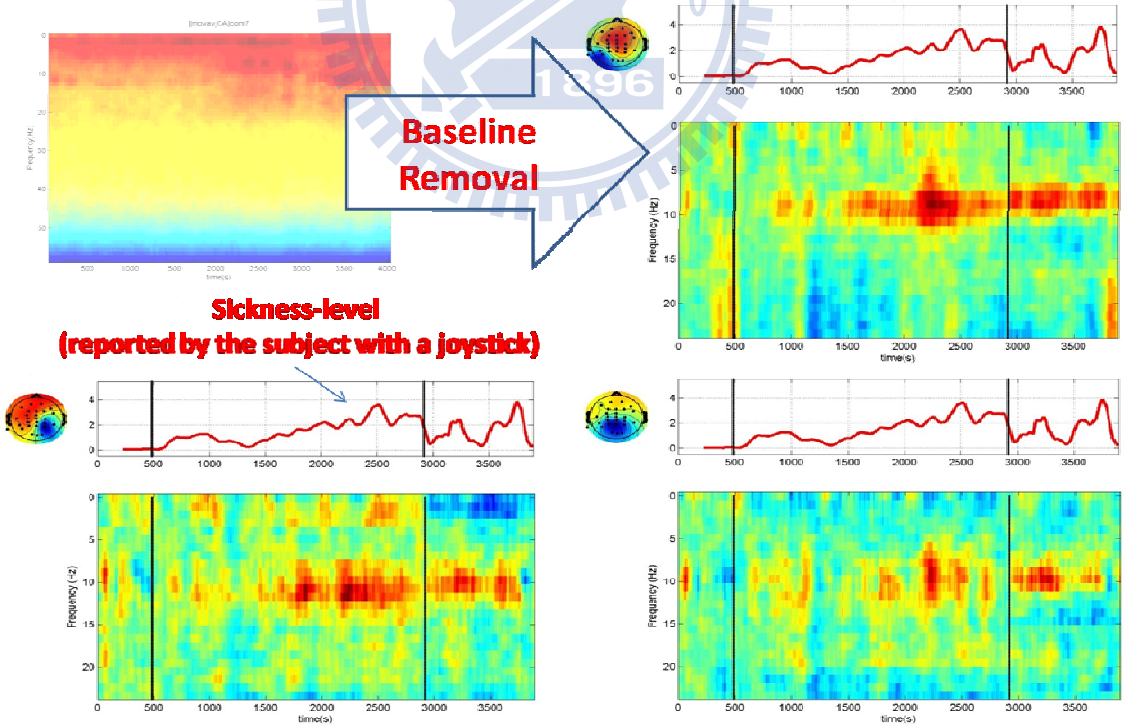

Fig. 2-8. Baseline removal of the time-frequency results.

MS-sorted EEG spectra

To examine the relationship between the severity of motion-sickness and concurrent changes in the EEG spectrum, the EEG power spectra were first computed in the winding-road section, and the spectra were sorted by subjective MS level for each of the component. The sorted EEG spectrogram at each MS level was then averaged across the components within each IC cluster. Linear regression was used to determine if the spectral changes vary as a function of MS level.

Time Relationship among MS-related EEG Processes

Multiple components exhibited MS-related spectral changes. The time relationship between these EEG processes is of interest. A cross-correlation analysis was performed on the power spectra of selected ICs for each individual. To be more specific, the spectrogram at each frequency were temporally shifted from -200 to 200 s with a step size of 1 s and correlated with the time series of the subject's MS ratings. Finally, the results were averaged across components in each of the five IC clusters.

2.4.2 Analysis of ECG Signals

The HRV was analyzed according to the modified procedures developed by Camm et al. (Fig. 2-9) (Camm et al., 1996; Kuo & Yang, 2002). Briefly, the (QRS) peaks

were first identified in the digital ECG signals using spike-detection algorithms (Fig. 2-9 A) (Kuo & Chan, 1992). The QRS rejection procedure was then utilized to remove the irregular QRS complex resulting from noise or un-related behavioral responses. For each heartbeat, this procedure evaluated the amplitude of the Q-R wave (AQR), amplitude of the R-S wave (ARS), duration of the Q-S wave (TQS), and duration of the R-S wave (TRS). Each heartbeat was then scored based on the values of these 4 indices compared to the mean and standard deviation (SD) of each of these 4 indices. If an index of a heartbeat fell within the range of its mean ± 4 SD, this heartbeat was assigned 1 point. Hence, these 4 indices were summed as the final score for each heartbeat in a range of 0 – 4. A heartbeat with a final score < 3 was discarded as noise.

The temporal position of the R peak for each valid QRS complex (screened by the above-mentioned procedures) was defined as a heartbeat, and the interval between two successive R peaks (R-R interval) was calculated from the time series of R peaks. The normal R-R interval is 0.5 – 1.3 sec (Grossman et al., 2004; Roach et al., 2004). The R-R intervals outside this range (or mean ± 3 SD) were eliminated from further analysis. The validated R-R values were subsequently resample and interpolated at the rate of 250 Hz to preserve the continuity in time domain. The heart rate (HR) measures the number of heartbeats taken per minute and the formula for calculating

the HR is 1 divided by averaged R-R interval of one minute (Olufsen et al., 2008). We adopted a 5-min overlapping window advancing at a 0.5-min step to calculate HR from R-R interval and then performed the time averaging (Matlab Curve Fitting Toolbox, function “smooth” with a moving setting of 25). The R-R interval of whole experiment was subjected to the fast Fourier transform (FFT) with a 5-min Hamming window overlapped by 4.5 min. Thus the temporal resolution of the HRV indices was 30 second. This study focused on three frequency bands: the VLF (0.003 – 0.04 Hz), LF (0.04 – 0.15 Hz), and HF (0.15 – 0.4 Hz) (Fig. 2-9 C) (Camm et al., 1996; Kuo et al., 1999). The powers of the LF and HF were normalized by total power minus the power of the VLF, representing components in normal units (NLF and NHF); that is, NLF = LF / (total power − VLF) * 100% and NHF = HF / (total power − VLF) × 100%, where total power = LF + HF + VLF. The natural logarithmic transformation only applied on the LF/HF ratio, that is, LF/HF ratio = log (LF/HF). The time series of the NLF, NHF, and ratio of LF to HF were then time averaged (Matlab Curve Fitting Toolbox, function “smooth” with a moving setting of 25) (Fig. 2-9 E).

To assess the changes in HRV indices (NHF, NLF and LF/HF ratio) under different degrees of MS, this study first defined the periods of low, high, and recovery MS levels. The high MS level window was defined as the period during which a subject’s MS rating was 75 – 100 % of maximum MS. The low MS level window was defined

as the period with the same length as the high MS level window, but low MS level window started from the beginning of the baseline session; conversely, the recovery MS level window was defined as the same length as high MS level window prior to the end of the recovery session. For instance, if *d* min is required for the MS level to increase from 75% to 100% of the maximum value, the low MS level window was then defined as the first d min of the baseline session, whereas the recovery MS level window was defined as the last d min of the recovery session. The window lengths varied from 1 to 16 min across 35 subjects and the mean of the window length is 7.12 ± 4.5 min. Consequently, the window length varied among subjects. The HRV indices derived from ECG signals in the three windows were statistically compared.

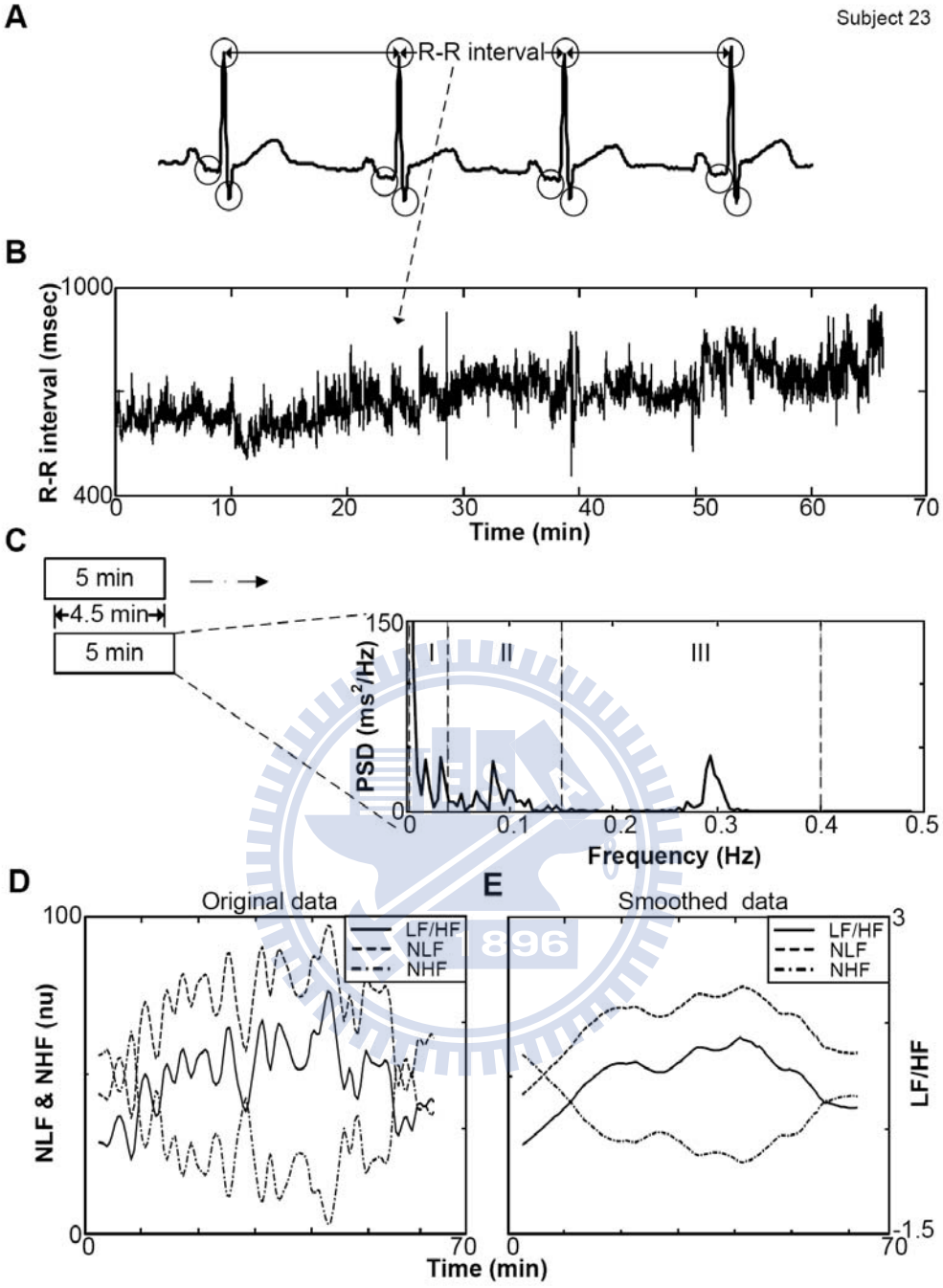

Figure 2-9. A schematic representation of the method used for spectral analysis of HRV for 1 subject. (A) The surface electrocardiogram. (B) A Matlab program is used to detect QRS peaks, compute individual R-R intervals and save the results as the tachogram. (C) Three major components: very low frequency (VLF, I), low frequency (LF, II). (D) The tachogram is subjected to FFT with a 5-min Hamming window, overlapped by 4.5 min and high frequency (HF, III), are derived from the power spectrum density (PSD) of R-R intervals. (E) The time series of HRV indices are then smoothed using the Matlab function "smooth" (Matlab Curve Fitting Toolbox).

Adaptive neural fuzzy inference system (ANFIS)

The ANFIS is a class of adaptive multi-layer feed-forward neural networks that are functionally equivalent to fuzzy inference systems. The ANFIS is typically used to formalize a systematic approach to generating fuzzy rules from an input-output dataset. The parameters for training the fuzzy inference system (FIS) membership function were determined by the ANFIS and using the Matlab function "anfis" (Matlab fuzzy logic toolbox). Given an input/output dataset, the "anfis" function constructs an FIS whose membership function parameters are adjusted using the back propagation algorithm with a least squares method (Jang, 1991; 1993). This allows the FIS to learn from input data. The procedure is briefly described as follows. First, the Matlab function "genfis1" (Matlab fuzzy logic toolbox) generated a Sugeno-type FIS structure (Jang *et al*., 1997) as the initial conditions (initialization of membership function parameters) for the function "anfis". Equation 1 shows a common Sugeno-type FIS structure.

$$\begin{aligned} &Rule1: if \quad x_1 \quad is \quad A_1, and \quad x_2 \quad is \quad B_1, then \quad f_1 = \alpha_1 x_1 + \beta_1 x_2 + \gamma_1 \\ &Rule2: if \quad x_1 \quad is \quad A_2, and \quad x_2 \quad is \quad B_2, then \quad f_1 = \alpha_2 x_1 + \beta_2 x_2 + \gamma_2 \end{aligned} \tag{1}$$

For the "anfis" function, the generalized bell-shaped built-in membership function "gauss2mf" (Matlab fuzzy logic toolbox) was adopted with 2 membership functions. The input matrix of training data included input data (smoothed NLF, NHF, and

LF/HF ratio indices) and output data (smoothed MS levels). When the functions "genfis1" and "gauss2mf" were defined, the "anfis" function started training. The parameters associated with membership functions were updated during the learning processes. The convergence of these parameters (or adjustments) was facilitated by a gradient vector, v_{ij}. This gradient vector assessed how well the FIS modeled data for a given set of parameters. When the gradient vector was acquired optimization, routines in Eqs. (2) – (4) were applied to adjust parameters to reduce error (E). Error (E) was defined as the sum of squared differences between actual output f and desired output y_d.

$$E = (y_d - f)^2 \tag{2}$$

$$\Delta v_{ij} = -\eta \frac{\partial E}{\partial v_{ij}} \tag{3}$$

$$v_{ij}(h+1) = v_{ij}(h) + \Delta v_{ij}(h) \tag{4}$$

where v_{ij} was used to adjust parameters, with a step of Δv_{ij}.

The "anfis" function used back propagation in combination with least squares estimation to estimate membership function parameters. The parameters for the FIS were set according to a minimum training-error criterion. Output variables for the FIS were estimated by fuzzy inference calculation function "evalfis" (Matlab fuzzy logic toolbox), which has two arguments, including parameter "fis" and a training dataset.

Statistical analyses

The repeated measures ANOVA was utilized to test the significant differences among HRV indices (smoothed NLF, NHF, and the LF/HF ratio indices) under different MS levels (low, high and recovery MS level periods). The least significant difference (LSD) test was used as the post hoc test. Spearman's rank correlation coefficient was analyzed to determine the associations between changes in individual HRV indices (continuous NLF, NHF, and the LF/HF ratio) and the subjective MS levels. The Spearman's rank correlation coefficient was also utilized to test the significance of the correlations between self-reported MS levels and estimated MS levels by ANFIS. The averaged correlation coefficients between subjective MS levels and estimated MS levels by ANFIS across the 35 subjects are calculated by first applying the Fisher's *z*-transform to normalize the distribution, then taking the mean of the transformed cross-correlations, and finally applying the inverse Fisher's *z*-transform (Fries, 2001). The significance level was $p < 0.05$.

3 Results

3.1 Motion-Sickness-Related ECG Responses

3.1.1 MS levels and HRV indices over time

Figure 3-1 A shows the time course of the MS levels of a single experiment from the representative subject (subject 23). A phasic change in MS levels was induced by the dynamic VR-based tunnel scenes. The MS level of the subject (Fig. 3-1 A) was kept at 0 during the initial 10 min of the baseline straight-road session. The MS level then steadily increased starting from the 1st min and peaked at the 28th min after entering the winding-road session. The MS level showed that after about minute 38 the MS started to decline and was at the lower level by the start of the recovery session. The onsets of increasing MS varied across subjects. In average, the occurrence of maximal MS levels was at around 44 ± 8 min.

Although the exact temporal profile of MS levels varied among subjects, the group trend of temporal change in MS levels in general resembled that one of the illustrated subject (subject 23, see the supp. Fig. 3-1 A). These experimental results demonstrated that a dynamic VR environment can effectively induce MS. Moreover,

among 29 subjects, MS severity increased progressively after VR scenes switched to the winding-road session, and then decreased, but most of them did not return to the baseline level, after the VR session switched back to the recovery straight-road session, suggesting a residual effect.

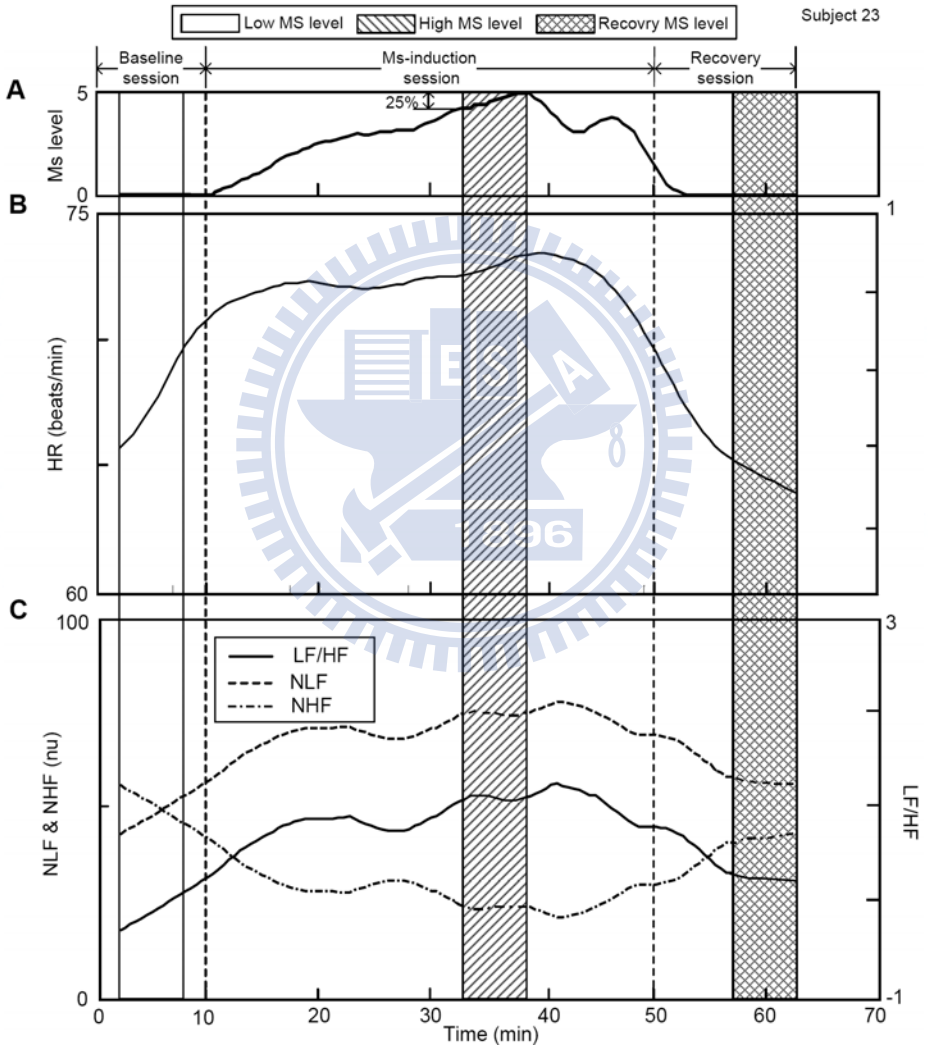

Fig. 3-1 Changes in MS level, HR and HRV indices during the driving experiment. (A) The time course of the self-reported MS for a typical subject (subject 23). (B) The HR of the subject during the driving experiment. (C) The smoothed NLF (dashed line), NHF (dash-dotted line) and the LF/HF ratio (solid line) of the subject during the driving experiment. .

Figure 3-1 (B and C) shows the changes in the HRVs (smoothed NLF, NHF and LF/HF ratio index) and the HRs over the entire experiment for the subject (subject 23). The NLF, LF/HF ratio and HR increased progressively as the experiment proceeded to the MS-induction session while the NHF generally decreased. During the recovery session, the NLF, LF/HF ratio and the HR decreased while the NHF increased as the MS level gradually returned to the baseline.

Figure 3-2 compares the mean of MS levels, HRV indices and HRs across 29 subjects under low, high and recovery MS level periods. The reported MS levels during recovery MS level period were significantly lower than those during the high MS level period (MS level, 0.79 ± 1.00 *vs*. 3.45 ± 1.31, $p < 0.001$; by the LSD tests), but higher than the values during the low MS level periods (Fig. 3-2A; MS level, 0.79 ± 1.00 *vs*. 0.03 ± 0.07, $p < 0.001$; by the LSD tests).

Figure 3-2 B compares the mean HRs of the subjects (n = 29) under low, high and recovery MS level periods. The mean HR varied significantly in these three different MS level periods (HR: $p < 0.001$, $F(2,56) = 23.20$, $\eta 2 = 11.52$; by the repeated measures ANOVA). The mean HRs during the recovery MS level period were significantly lower than those during the high MS level period ($p < 0.001$; by the LSD tests) and the low MS level period ($p < 0.05$; by the LSD tests).

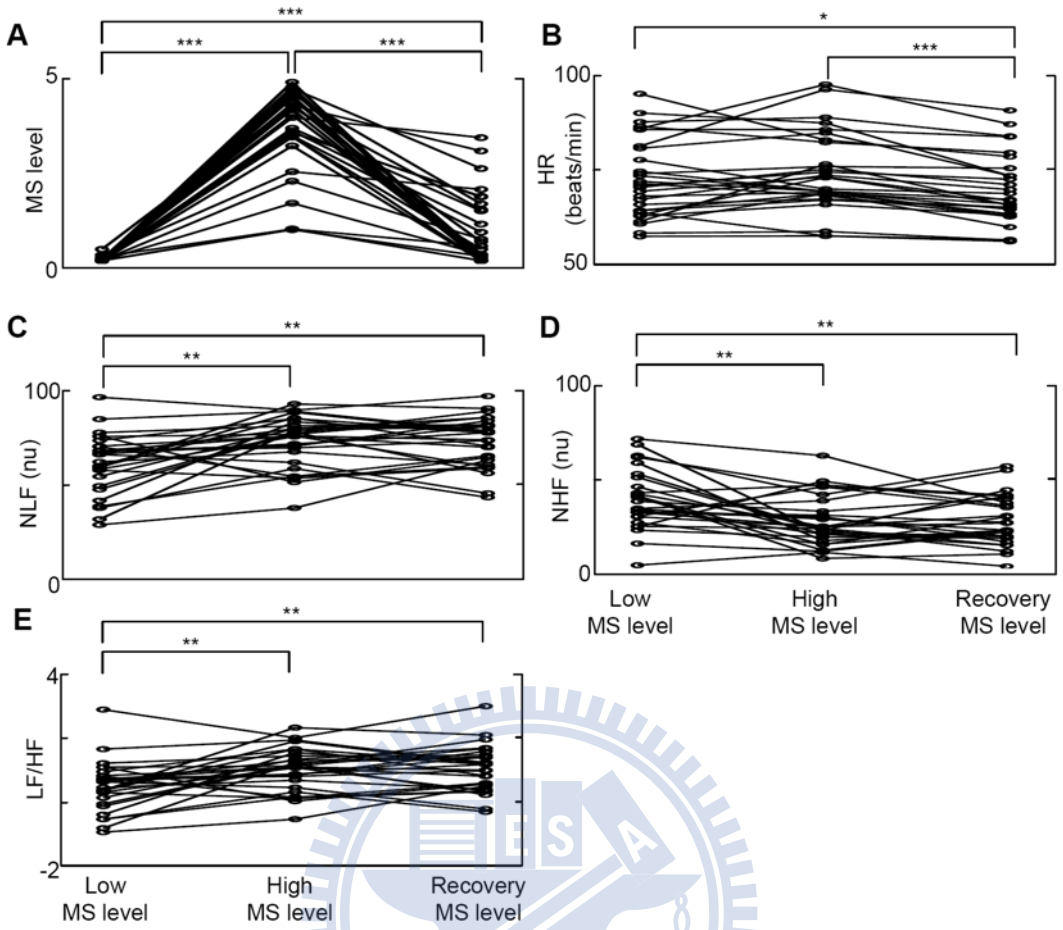

Fig. 3-2. Averaged (A) MS level, (B) HR, (C) NLF, (D) NHF, and (E) LF/HF ratio during low, high and recovery MS level periods for 29 subjects. Each circle represents the value of single subject. Statistical analysis results were noted as: * $p < 0.05$; ** $p < 0.01$; *** $p < 0.001$

Figure 3-2 C and E) compares the HRV indices during low, high and recovery MS level periods. The HRV indices varied significantly in these three different MS level periods (NLF: $p < 0.001$, $F(2,68) = 10.16$, $\eta 2 = 0.30$; NHF: $p < 0.001$, $F(2,68) = 10.16$, $\eta 2 = 0.30$; LF/HF ratio: $p < 0.001$, $F(2,68) = 9.87$, $\eta 2 = 0.29$; by the repeated measures ANOVA). Based on the difference between low and high MS level periods, subjects had statistically significant increases in averaged NLF and the LF/HF ratio

and significant decreases in averaged NHF values (NLF, $p < 0.01$; LF/HF ratio, $p < 0.01$; NHF, $p < 0.01$; by the LSD tests). No statistical difference existed in the averaged HRV indices between the high and recovery MS level periods (Fig. 3-2). The NLF, LF/HF ratio and NHF during the recovery MS level period were either higher or lower than those during the low MS level period.

However, the mean HRV indices of few subjects (n=6, defined as atypical subjects) was significantly different from those of the majority subjects (n=23, defined as typical subjects) during the low MS level period. The atypical subjects had significant higher NLF and LF/HF and lower NHF values than those of typical subjects. (NLF: $p < 0.05$, $F(1,27) = 5.34$; NHF: $p < 0.05$, $F(1,27) = 5.34$; LF/HF ratio: $p < 0.05$, $F(1,27) = 6.26$; by the repeated measures ANOVA). Furthermore, atypical subjects had decreases in the averaged NLF and LF/HF ratio, and increase in the averaged NHF values in terms of the difference between low and high MS lever periods. The NLF, LF/HF ratio and NHF within the recovery MS level window varied widely (either higher or lower than those during the low MS level period).

3.1.2 Correlations between HRV indices and MS levels

To quantitatively assess the correlation between changes in NLF, NHF, LF/HF ratio and MS levels over time, this study utilized the Spearman's rank correlation

coefficient to test the significance of the correlations between changes in individual HRV indices and self-reported MS levels. Results suggested that the mean correlation coefficient across 29 subjects between the individual HRV indices and the MS level did not match well (NLF, $r = 0.18$; NHF, $r = -0.16$; LF/HF ratio, $r = 0.18$). Thus the temporal profiles of the NLF, LF/HF ratio and NHF were only weakly correlated with MS levels.

3.1.3 Relationship between time-related changes in autonomic nervous function and MS levels

The Spearman's rank correlation coefficient indicate that temporal changes to MS levels are not significantly correlated with either the NLF index or NHF index of HRVs, as the latter represents vagal control and the former represents sympathovagal activities. However, the results of the correlations did not rule out the possibility that changes to MS levels may be reflected by the combination of sympathetic, parasympathetic or their balanced effects. To test this possibility, this study assessed the relationship between changes to MS levels and overall autonomic activities using an ANFIS. Figure 3-3 presents the actual and estimated MS levels obtained by ANFIS for subject 23 and the MS levels estimated matched well with the actual MS levels (r = 0.96), Table 1 shows the correlation coefficients for the correlation between the actual and estimated MS levels obtained by ANFIS for all 29 subjects by Spearman's

rank correlation coefficient. The mean correlation coefficient across subjects between MS estimated by the ANFIS and actual MS levels is 0.83. These analytical results demonstrate that continuous MS levels better correlated with a non-linear linear combination of HRV indices than with individual indices, suggesting a coupling of the sympathetic and parasympathetic activations or their balanced effects.

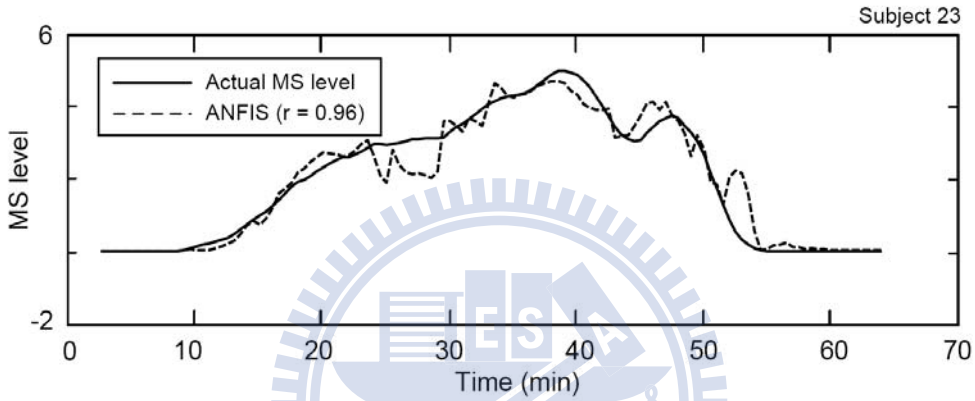

Fig. 3-3. The time courses of actual MS level (solid lines) and estimated MS levels obtained via an adaptive neural fuzzy inference system (black dashed line) methods for a typical subject (subject 23).

Table 1. Correlation coefficients between actual and estimated MS levels obtained by an adaptive neural fuzzy inference system (ANFIS) method.

Subject number	Correlation
	ANFIS
1	0.86
2	0.78
3	0.65
4	0.85
5	0.80
6	0.89
7	0.93
8	0.73
9	0.88
10	0.85
11	0.61
12	0.76
13	0.92
14	0.71
15	0.84
16	0.72
17	0.72
18	0.87
19	0.83
20	0.65
21	0.65
22	0.75
23	0.96
24	0.90
25	0.95
26	0.69
27	0.63
28	0.93
29	0.69
mean	0.83

3.2 Motion-Sickness-Related EEG Responses

ICA was separately applied to the EEG data from each subject, after bad channels and periods of data that contained disallowed or uncharacteristic artifacts were removed, to decompose the data into spatially fixed and temporally independent components. DIPFIT2 routines from EEGLAB were used to fit either one or sometimes two nearly bilaterally symmetric dipole source models to the component scalp topographies using a four-shell spherical head model (Oostendorp & Oostenveld, 2002). ICs were then clustered according to correlations among their dipole locations, time-frequency characteristics and overall power spectra.

Figure 3-4 shows the equivalent dipole source locations and mean and individual scalp maps for five MS-related clusters from 19 sessions. These clusters had equivalent dipole sources in the left motor (n=13), the parietal (n=11), the right motor (n=11), the occipital (n=14) and the occipital midline (n=12) areas. The two occipital IC clusters are separated based on the fact that the source locations of the occipital midline ICs are deeper than those of the occipital ICs.

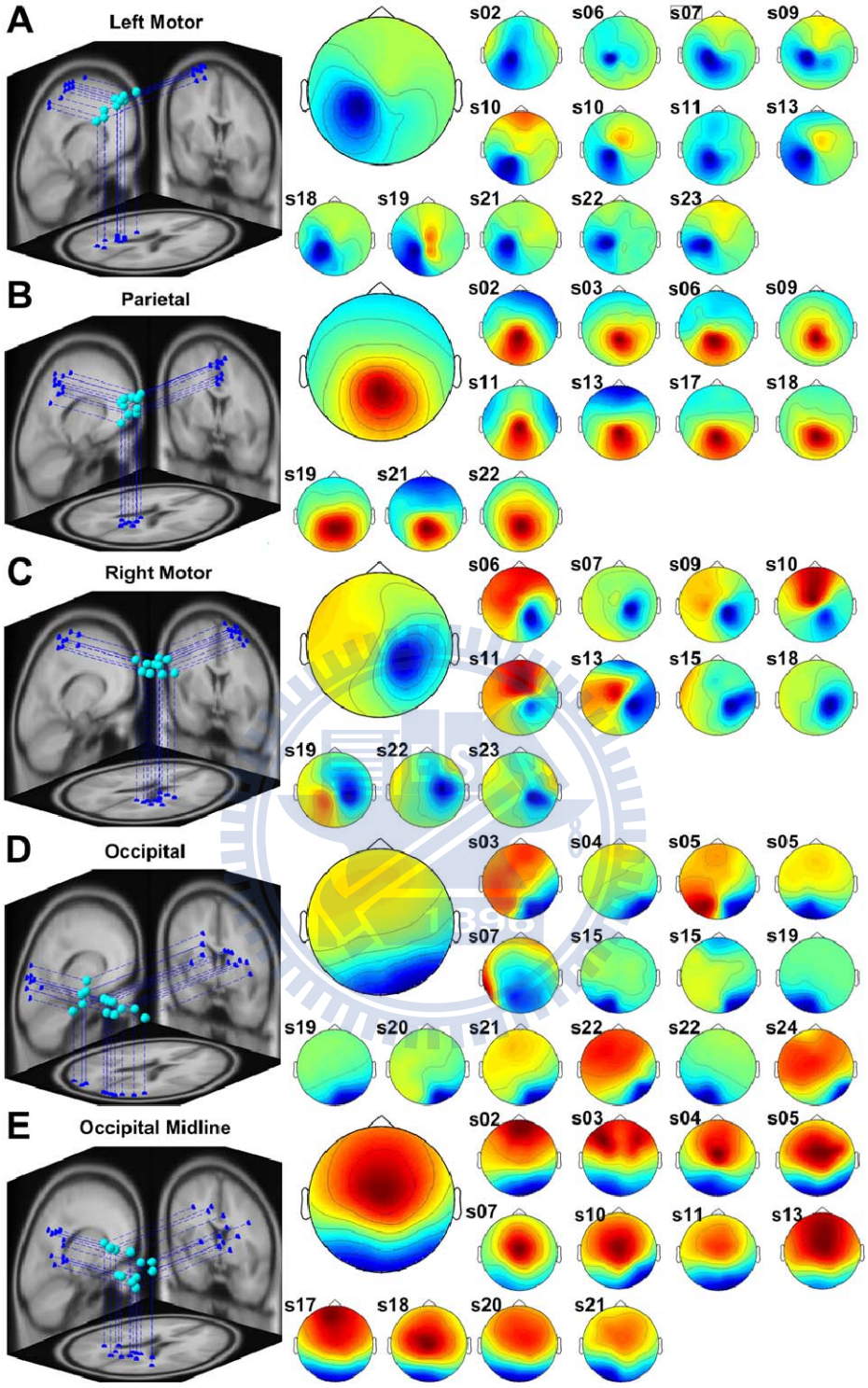

Fig. 3-4 Equivalent dipole source locations and mean and individual scalp maps for five IC clusters from 19 sessions. The 3D dipole source locations and their projections onto average brain images were given in the left panels. The single-subject scalp maps within each cluster and the averaged scalp maps were shown in the right panels. (A) left-motor (n=13), (B) parietal lobe (n=11), (C) right-motor (n=11), (D) occipital (n=14) and (E) occipital midline (n=12).

3.2.1 Spectral Changes under Different Conditions

Figure 3-5 compares the mean component power spectra of the IC clusters under different motion-sickness levels and various road conditions. The EEG spectral difference associated with the different road conditions is observed by elucidated the baseline power spectra (green traces in Figs. 3-5 B-F, from the very first 200 seconds of the baseline section) and the low-MS level spectra (blue traces, from the first 200 seconds of the curve-road section). Evidently, the alpha power of the right, left motor and the parietal components were suppressed from the straight-road driving to the winding-road driving as the car swayed from side to side. This finding suggests that these brain networks may be highly responsive to the movements of the platform and, hence, to somatic sensation. Further, the occipital midline IC cluster exhibited significant alpha power suppression (Fig. 3-5F).

Comparing the component power spectra under low MS level (blue traces in Fig. 3-5) and high MS level (red traces, 200 seconds period starting from the peak MS rating) revealed MS-related spectra changes. The red asterisks in Fig. 3-5B-F indicate the frequency bins where the component EEG power differed significantly between the maximum and minimum sickness levels under the same curve road condition ($p<0.01$, the paired-sample Wilcoxon signed-rank test). The alpha power of the occipital IC cluster (Fig. 3-5E) increased significantly with the MS level, whereas the

occipital midline component cluster exhibited broadband spectral elevation at high MS. This result was perfectly in line with the results reported by Klimesch and colleagues (Klimesch, 1999; Klimesch et al., 1998).

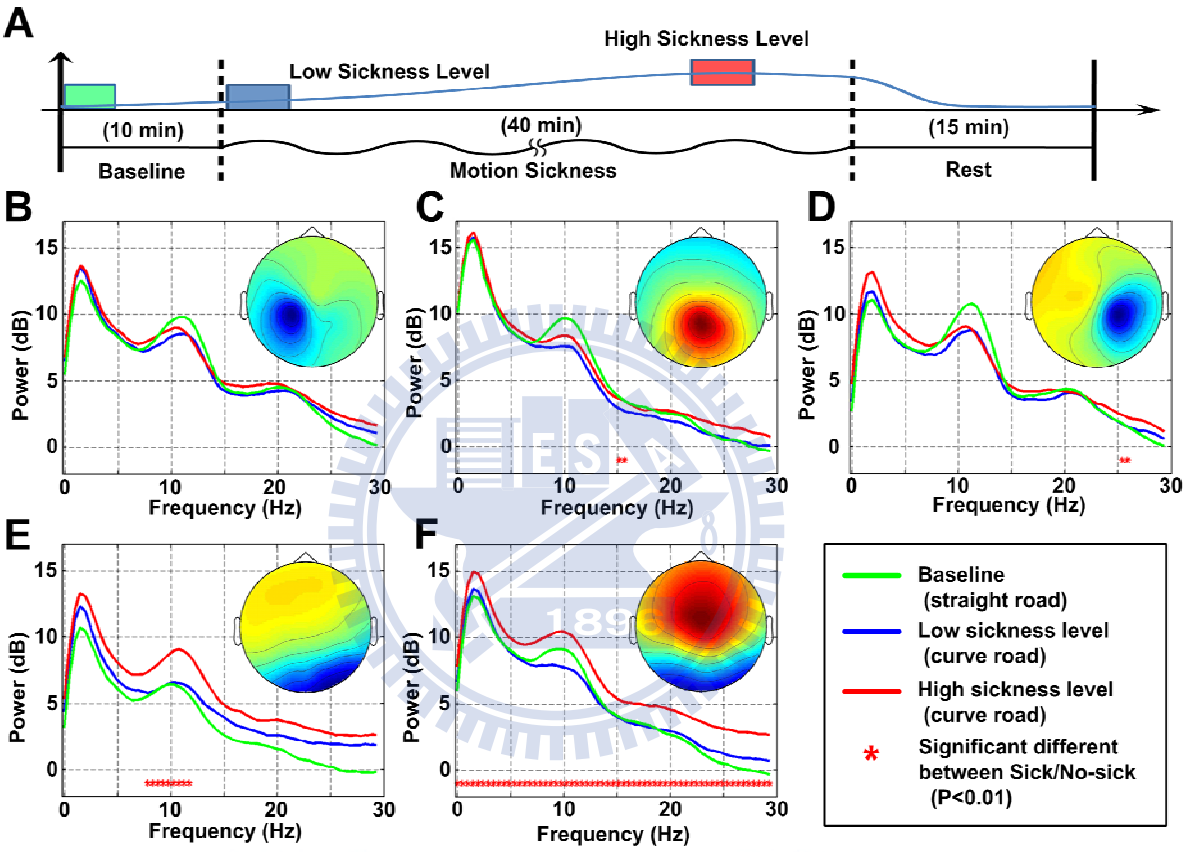

Fig. 3-5. Comparison of ICs' power spectra comparison under different motion-sickness levels and various road conditions. The averaged ICA power spectra of baseline (straight-road / no-sick) were shown as green lines, the power spectra of low sickness level (curve-road/ no-sick) were shown in blue lines, and the power spectra of high sickness level (curve-road/ sick) were shown in red lines. The red asterisks indicated the frequency bins where the component EEG power differed significantly between the maximum and minimum sickness levels under the same curve road condition ($p<0.01$, the paired-sample Wilcoxon signed-rank test).

3.2.2 Single-subject Motion-sickness-related Time-frequency Responses

Time-frequency analysis was adopted to evaluate EEG correlates of fluctuations of MS level for the five selected IC clusters. Figure 3-6 plots the time-frequency response of three ICs - the occipital, parietal and right motor components - from one of the 19 subjects. The time-frequency responses of these three ICA components were evidently related to MS across time. Among these ICs, the correlation between the MS level and the changes in the alpha power in the occipital area (Fig. 3-6B) was the most pronounced. Furthermore, the changes in the alpha power in the parietal and the motor areas were also correlated with the MS levels (Figs. 3-6C and D).

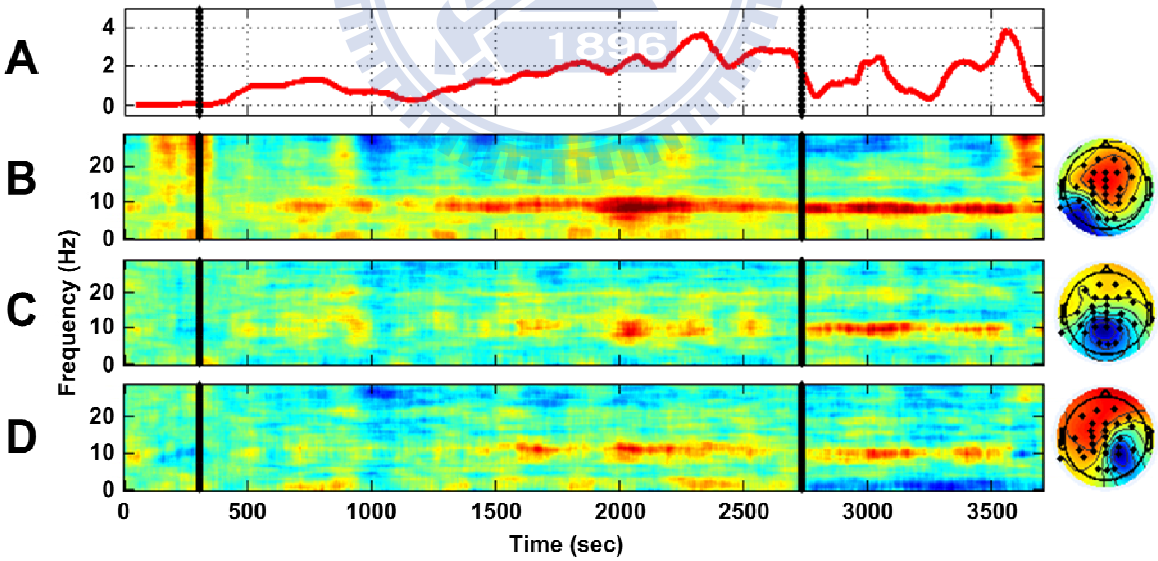

Fig. 3-6. Single-subject time-frequency results in the occipital, the parietal and the right motor components from one of the 19 subjects. (A) The recorded sickness level was shown in red. (B-D) Time-frequency responses of three ICA components co-varied with MS level at several frequency bands.

3.2.3 Group MS-related Spectral Changes

To study the group EEG correlates of MS across subjects, the time-frequency responses of each subject were sorted first by level of motion-sickness; the sorted time-frequency responses were then averaged across subjects. Figure 3-7 plots the averaged group time-frequency responses that accompanied motion-sickness for the five component clusters. The 3D plots reveal that the EEG power changes from low- to high- MS levels (1 to 5). The lower left 2D figures plot the net effects of MS on the spectra in different brain areas, obtained by subtracting the EEG power at low MS from the total EEG power in the 3D plots. Finally, a regression line was used to represent the linear relationship between the changes in EEG power and motion-sickness. The gradient reveals the way in which MS level mediated the EEG power.

The left motor area (Fig. 3-7A) exhibited predominant spectral increases in all frequency bands as the MS level increased. The theta power increased by 3 dB, while the alpha and beta power increased by about 2 dB from the low-MS (1) to high-MS (5) state. The power spectra of the parietal components (Fig. 3-7B) increased in the delta, theta and alpha bands, while the beta-band power decreased by 2 dB as the MS level increased. The theta-band power increased by more than 5 dB in the right motor area (Fig. 3-7C) while the alpha-, delta- and beta-band power also increased slightly as the

MS level increased. The occipital components (Fig. 3-7D) also exhibited significant (more than 5 dB) spectral increases in the delta and theta bands. Increases in the broadband power spectra were observed in the occipital midline components, as presented in Fig. 3-7E.

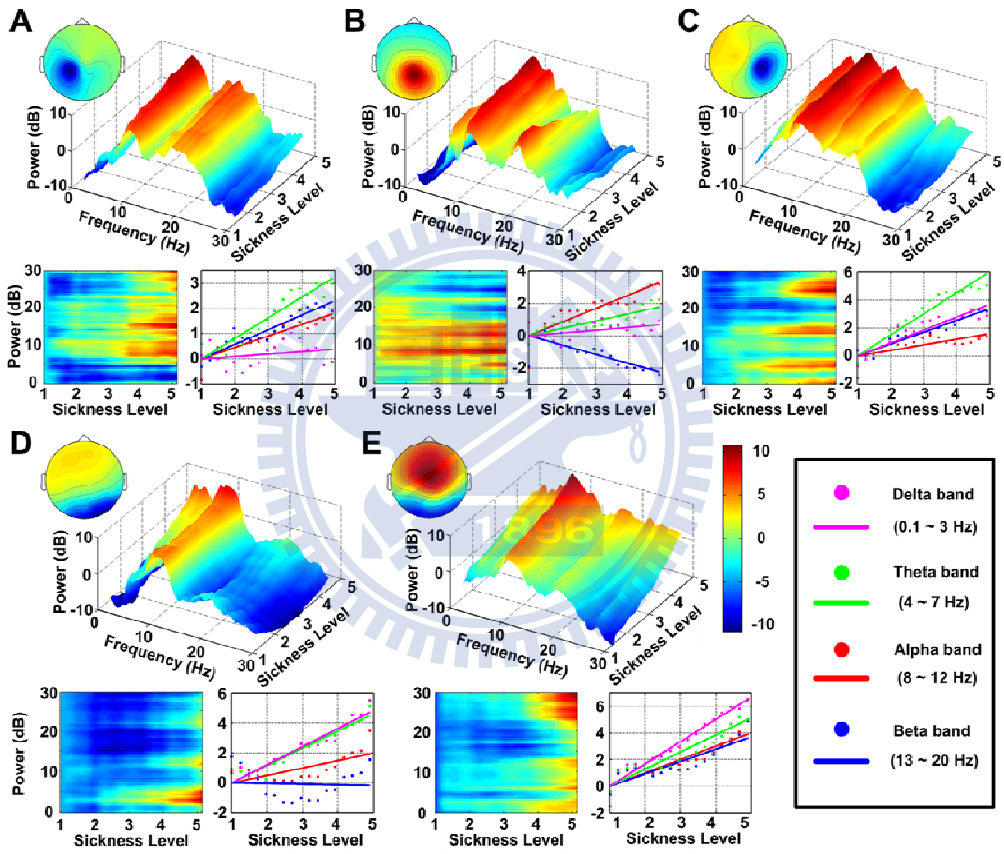

Fig. 3-7. The averaged group time-frequency responses during motion-sickness for the five component clusters. The time-frequency responses of each IC were first sorted according to the sickness level. The sorted sickness-related time-frequency responses within each cluster were then averaged and plotted in the 3D plots. The 3D plots reveal that the EEG power changes from low- to high- MS levels (1 to 5). The lower left 2D figures plot the net effects of MS on the spectra in different brain areas, obtained by subtracting the EEG power at low MS from the total EEG power in the 3D plots. The show the linear trends of the EEG power changes in different frequency bands against the motion-sickness levels. A regression line was used to represent the linear relationship between the changes in EEG power and motion-sickness. The gradient shown in lower right panels reveal the way in which MS level mediated the EEG power.

3.2.4 Time Relationships between Motion-sickness-related Brain Processes

Figure 3-8A presents the overall correlations between the component spectra and their corresponding MS levels of the seven clusters. The correlation coefficients in the alpha band exceed those in other frequency bands in MS-related clusters. The maximum correlation coefficient in the alpha band is 0.5 in the occipital midline components, while the correlation coefficients are approximately 0.4 in other IC clusters. In addition, the maximum correlation coefficient between the time courses of the two eye-movement components and the MS-level is 0.2.

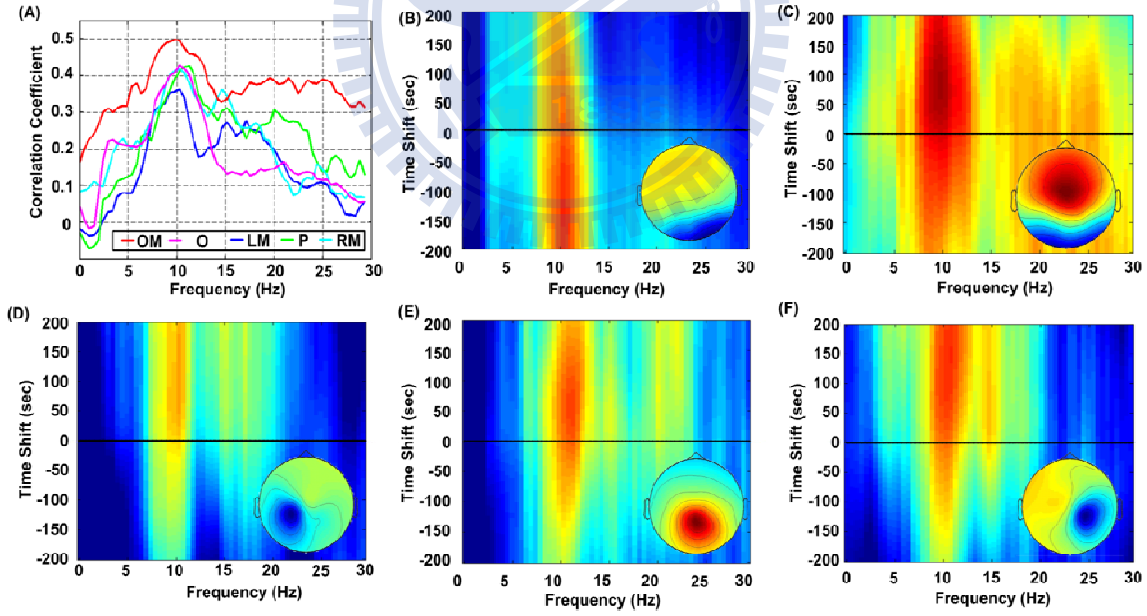

Fig. 3-8. The results of correlation and cross-correlation analysis between subjective sickness level and ICA power of the five brain areas. (A) The overall correlations between the component spectra and their corresponding MS levels of the five clusters. (B-F) The time relationships between the MS-related EEG processes of the five independent clusters.

The time relationships between the MS-related EEG processes were computed and displayed in Figs. 3-8 B-F. The highest correlation coefficients in the somatosensory areas (Fig. 3-8D and F) in the alpha band were obtained by shifting the sickness-level signals backward by approximately 100 s. The highest correlation coefficients of the parietal (Fig. 3-8E) and occipital midline (Fig. 3-8C) in the alpha band were obtained by shifting the behavior signals backward by about 80 and 60s, respectively, whereas the highest correlation coefficients of the occipital (Fig. 3-8B) in the alpha band were obtained by shifting the sickness-level signals forward by about 120s.

The results suggest that the independent EEG components can be used to predict the onset of motion-sickness. Some of them preceded the subjects' sickness ratings, such as the alpha power in the somatosensory areas, which fact might reflect the suppression of vestibular inputs to eliminate the conflict with subjects' visual perception. Then, at approximately 60 s before subjects reported their motion-sickness, the occipital midline area began to exhibit the MS-related alpha power increases. Moreover, this independent component exhibits the strongest correlation with the motion-sickness rating. Consequently, this IC cluster may be a potential index to predict the onset of motion-sickness.

4 Discussions

4.1 Motion-Sickness-Related ECG Responses

4.1.1 Correlations between HRV indices and MS levels

This study demonstrates that HRV indices derived from recorded ECG signals during low MS level period were significantly different from the ones derived in the high MS level period. This experimental results also indicated that autonomic control is involved in the development of MS symptoms, and is consistent with those of previous studies showing that exposure to motion sickness stimulation increases cardiac sympathetic and decreases cardiac parasympathetic activities, as reflected in HRV (Holmes & Griffin, 2001; Yokota *et al*., 2005). However, Ohyama *et al*. (2007) reported that during exposure to a VR environment, MS induced increasing sympathetic activity without vagal changes. The discrepancy between their experiment and the current study might be the different methods used to assess MS levels and the indices used to evaluate autonomic function. This study used normalized rather than raw powers to index HRV. Such indices are proven to best reflect sympathetic and parasympathetic responses (Yang *et al*., 2000; Arlt *et al*., 2003;

Chen *et al*., 2006). Furthermore, the slide-type switch used for subjects to rate their MS levels could contribute to the differences as well. The advantage of using switch for continuous rating was the subjects would not need to be interrupted by the researcher during the continuous experiment sessions. If the subject's MS level was scaled every minute by interrupting the experiment, the subject probably could get momentarily relief from the MS. In turn, the MS levels could be different from the continuous MS without interruption. As a result, the induced MS in this study would more resemble our real-world experience. Though we can't totally rule out that our method could potentially interfere with the subject's experience of MS, the interference in our method should be smaller than that of the methods used in previous studies and possibly be subtracted out from the behavioral and physiological data (Holmes & Griffin, 2001; Young, 2003; Ziavra *et al*., 2003).

A small number of subjects in this study had autonomic responses opposite to those of the majority of subjects during MS exposure. These atypical subjects (n = 6) likely failed to respond to VR stimulation. These subjects reported that they felt sickness immediately after the onset of the experiment. Such early onset sickness could be induced by the unfamiliar with the VR-scene. Previous studies have suggested that subjects first exposed to the VR scene could suffer from the cybernetic sickness (Morrow et al., 2002). Though subjects were required adapting to the VR scene for 10

min before the MS experiment in order to prevent the sickness induced by the VR scene, the results suggested that 10 min practicing time might not be sufficient for these 6 subjects to adapt themselves to the VR scene. The duration for adapting/training to the VR scene will be more appropriately determined on an individual-subject basis in the future study.

Results of a Spearman's rank correlation coefficient analysis showed that temporal changes in the MS levels did not correlate strongly with the alterations in individual HRV indices, indicating that no significant changes existed for individual HRV indices and self-reported MS levels. However, the non-linear combination of HRV indices modeled by ANFIS co-varied well with the self-reported MS levels. HRV indices represent the cardiac sympathovagal activists and its balance of autonomic nervous system which is properly maintained by the neural regulation of circulatory function in almost every second of our daily lives (Shanthi & Kumaravel, 2005; Tracey, 2007). The cardiac sympathetic and parasympathetic nerves have overlapped dynamic actions. The concept of the sympathovagal balance also suggests that the activation of either sympathetic or vagal outflow is always accompanied by the inhibition of the other activity, but there are the independent changes in sympathetic and parasympathetic in certain circumstances, e.g. co-activation, co-inhibition, etc (Zhong et al., 2006; Hermans, 2006; Lenneman & Backs, 2007). This reciprocal

organization seems instrumental to the fact that sympathovagal excitation are both presumed to contribute to the increase or decrease of cardiac performance required for various behaviors **(**Montano et al., 2009**)**. Furthermore, the sympathovagal activities and its balance were highly disturbed by the exposure to provocative stimulation such as the MS induction (Gianaros et al., 2003; Emoto, 2008). On the other hand, several studies suggested that MS symptoms were probably induced by prolonged disturbance of the sympathovagal modulations and their balance (Doweck et al., 1997; Finley et al., 2004) and such disturbances could be reflected by the cardiac sympathovagal activities (Morrow et al., 2000; Yokota et al., 2005; Ohyama et al., 2007; Emoto et al., 2007; Emoto, 2008). Therefore, the combined HRV measures, which included the sympathetic and parasympathetic activities as well as the sympathovagal balances, could better model the fluctuations of MS levels than the individual HRV indices alone.

Several previous studies also indicated that no correlation existed between self-reported MS symptoms and power spectra of HRVs. They suggested that this was due to large inter- and intra-subject variability of self-reported MS and proposed that a non-linear relationship exists between perception and sensitivities to MS (Bos & Bles, 1998; Beckers et al., 2006; Peng *et al*., 2007; Arribas & Piñeiro, 2007; Ohyama *et al*., 2007). Other contributing factors may be that any particular HRV index may

not account for phasic changes in MS levels (Morrow *et al*., 2000; Collet *et al*., 2000; Levin *et al*., 2004; Yokota *et al*., 2005; Sugita *et al*., 2004). Hence, changes in MS levels over time would likely not correlate perfectly with autonomic responses. Such reciprocal timeity and feedback within dynamic systems is best modeled with nonlinear equations because nonlinearity allows interactive and bidirectional relations. This study demonstrates that a non-linear combination of HRV indices modeled by ANFIS co-varied well with changes in self-reported MS levels, indicating the coupling effects of sympathetic and parasympathetic activities on MS.

4.1.2 Correlations between Heart rate (HR) and MS levels

No significant change was found in the mean HR during the low and high MS level periods. We speculated that the net effects of ANS activities were not strong enough to predominately affect the HR even the increase of HR has known to be depended on the sum of the cardiac sympathetic and the parasympathetic activities (Yang et al., 2000). For example, the HR was increased when the cardiac sympathetic activity was dominant (Pumprla et al., 2002; Adamson et al., 2004) and the HR was slow down when the cardiac parasympathetic activity was dominant (Pierpont et al., 2000; Carter et al., 2003). The cardiac sympathetic and parasympathetic are also know to be activated at different temporal profile (Camm et al., 1996; Mrowka et al., 2000). The

activities of sympathovagal are highly variable during the MS induction because the MS symptoms were probably induced by prolonged disturbance of the cardiac sympathovagal modulations and their balance (Yokota et al., 2005; Emoto, 2008). Therefore, the net effects of cardiac sympathovagal activities in the HR are not as sensitive as the HRV indices to the increases of MS levels (Schlegel et al., 2001; Santarcangelo et al., 2008).

The similar net sympathovagal effects were found in HR during the recovery MS level period. The averaged HR was lower in the recovery MS level period than that in the low and high MS level periods. Most of the subjects had increases in the NHF and decreases in the NLF later during the recovery MS level period**,** suggesting that the parasympathetic activity was dominant during the recovery MS level period and its effect was also reflected on the decreased averaged HR. This finding is also consistent with the hypothesis that the HR recovery is related to the parasympathetic activity (Cole et al., 1999; Kannankeril et al., 2004; Yerdelen et al., 2008).

4.2 Motion-Sickness-Related EEG Responses

This study elucidates EEG correlates of motion-sickness in a realistic VR- and motion-platform-based driving simulator. The recorded EEG data of each subject were first decomposed using ICA to isolate the spatially fixed and temporally

independent EEG processes from the noise and artifacts. The time courses of spectral changes of these independent EEG components were then correlated with the subject's motion-sickness ratings that were simultaneously recorded during the experiment.

4.2.1 Modalities to Induce Motion-sickness

The sensory conflict theory proposes that motion-sickness may be caused by the receipt of incongruent information from the multi-modal somatosensory system, including visual information and most importantly, vestibular sensations. Thus, most studies in the field have introduced conflicting multi-modal somatosensory information to induce motion-sickness symptoms. Some have employed the rotary chair (Wood *et al.*, 1991; Wood *et al.*, 1994) or the parallel swing (Wu, 1992), which create bodily movement without corresponding visual cues, and further generated incongruent somatosenaory inputs. Others have adopted visual stimuli with no vestibular input, such as by using cross-coupled angular stimulation (Chelen *et al.*, 1993), the optokinetic drum (Hu *et al.*, 1999) or other forms of stimulation (Lo & So, 2001; Kim *et al.*, 2005; Min *et al.*, 2004), to induce motion-sickness symptoms. However, since motion-sickness involves the multi-modal somotosensory system, the incorporation of both visual and vestibular stimuli into the motion-sickness studies is more realistic. Combining a VR scene with a dynamic motion platform provides a

more complete environment in which to investigate the effect of the motion-sickness on cognitive states, as well as the underlying neurophysiology. In this study, this combined modality is used to induce near-real-world motion-sickness.

4.2.2 MS-related Spectral Changes

Figures 3-4 A-C reveal that the alpha power increases with the MS-level, especially in the parietal lobe. This result is consistent with the results of a gravitational experiment that was conducted by Cheron *et al.* (2006), who determined that 10Hz oscillations in the parieto-occipital and sensorimotor areas increased as gravity was removed. They also suggested that since the parietal lobe is situated at a transition between the somatosensory and the motor cortex, it may therefore be involved in the integration of spatial representation, which requires body sensation information from vestibular inputs.

In the right and left motor areas, the increases in the theta band power are greater than those in the delta, alpha and beta bands (Figs. 3-4 A and C). Such theta power increases have also been recorded in numerous studies of motion-induced motion-sickness. However, the brain areas that have been associated with the theta power increases are not completely consistent. Wu (1992) reported theta power increases in the frontal and central areas in a parallel swing study. Significant MS-related theta power increases have been induced in the frontal areas using a

rotating chair (Wood *et al.*, 1991; Wood *et al.*, 1994). However, Chelen *et al.* (1993) reported theta power increases in the temporo-frontal in a cross-coupled angular stimulation experiment.

The theta power increases can be referred to sensorimotor integration, which were demonstrated in a way-finding VR experiment by Caplan *et al.* (2003). They found theta oscillations in the peri-Rolandic regions and the temporal lobes were related to (1) movement (both virtual and real), (2) updating the motor plan according to the information collected from a multi-modal somatosensory system, and (3) coordinating with the internal map during navigation. However, in the experiment in this study, the subjects were instructed to report their motion-sickness levels using a joystick only. The subjects had to report no further navigation information (such as number and degree of turns and related information). Although the real turns may unavoidably influence navigation function of the subjects, their effect should be relatively limited. Moreover, the possibility of motion-induced theta power changes was eliminated by removing the EEG power changes that were related to the baseline under the two experimental conditions - baseline straight-road and baseline curve-road conditions. Consequently, the theta power increases found in the two motor areas were caused mainly by the integration of the multi-modal somatosensory information, which may be essential to the motor planning of bodily movement in response to the motion of

the platform during cruising on the curved road. Additionally, Caplan *et al.* (2003) claimed that the effect of the theta power increase was asymmetric across the left and right hemispheres. The power increase is more pronounced in the right hemisphere than in the left. The results herein were consistent with their findings (Figs. 3-2B and D). Bland & Oddie (2001) also developed the sensorimotor integration hypothesis, according to which theta oscillations act to coordinate activity in various brain regions to update motor plans in response to somatosensory inputs. Jensen (2001) demonstrated that theta oscillations act as carrier waves for information transfer between any pair of regions via synchronized oscillations at the same frequency.

In the occipital midline component cluster (Fig. 3-4E), component spectra monotonically increased with the MS level in all frequency bands (delta, theta, alpha and beta). Such a broadband power increase may indicate that motion-sickness can strengthen the underlying brain processes, perhaps because of the difficulty of the task during motion-sickness. This result may also indirectly demonstrate conflicts within multi-modal somatosensory systems as they sense the environment around the subject, causing the related brain circuits to work harder than at the baseline (no motion-sick condition). According to the results of the correlation analysis (Fig. 3-5A), in the occipital midline cluster, the EEG power responses in the occipital midline were more highly correlated to subjective sickness-levels than in other brain areas, suggesting

that activations in the occipital midline may be useful in determining the stages of motion-sickness.

Although determinations by various studies of the brain regions that are involved in motion-sickness remain inconclusive, many studies have presented delta power increases. For example, an increase in delta-band power was observed at C3 and C4 in an optokinetic rotating drum experiment (Hu *et al.*, 1999) and in the frontal and temporal areas in an object-finding VR experiment (Kim *et al.*, 2005). A delta power increase at Fz and Cz was also found in a VR-based car-driving experiment conducted by Min *et al.* (2004). Furthermore, a delta power increase has also been reported in a motion-induced motion-sickness study using cross-coupled angular stimulation (Chelen *et al.*, 1993). In that study, the delta power increase was detected over the occipital, the occipital midline, and the right motor IC clusters (Fig. 3-4 C, D, and E), mainly during the curved-road section (Fig. 3-3). This change in EEG power may be treated as a stress component caused by the motion-sickness or violent movement of the motion platform, as suggested by Chen *et al.* (1989).

The resultant spectral changes might be due to a confounding effect of moving a joystick and motion sickness. However, the joystick movements were very sparse as the subjects did not need to move the joystick unless they felt the level of motion sickness has been changed. Previous studies (Huang et al., 2007; Huang et al., 2008)

showed that the spectral changes following finger/hand movements in the sustained attention tasks were usually transient (a quick spectral suppression followed by an equal-amplitude rebound within 2-4 seconds). Furthermore, these spectral perturbations would be the same regardless if the subject reported an increase or a decrease in the sickness-level. Thus, the joystick movements would not have biased the spectral correlates toward to a spectral increase or decrease systematically when the correlation between the time course of component spectra and the subjective sickness level was calculated in a much longer (smoothed) time scale.

4.2.3 Time Delay

Cross-correlation analysis between the subjective sickness-level and the power spectra of the independent EEG components facilitates an investigation of the underlying neurophysiology of motion-sickness in the human brain. Our analysis results revealed a strong positive cross-correlation of the subjective sickness level with spectra at 10 and 15 Hz of the two motor IC clusters, leading the peak of the subjective MS rating by 100s, possibly indicating the difficulty of integrating multi-modal somatosensory information into the motor-planning process or compensation of the movement of the motion platform, resulted in the suppression of the bilateral motor control-related brain circuits. However, a strong cross-correlation

existed with the alpha and beta spectra in the parietal and the occipital midline areas, leading the MS rating peaks by 80 and 60 s, respectively (Fig. 3-5 C and E). This finding may correspond to the extra loading associated with the integration of multi-modal somatosensory information during motion-sickness and the "perception" that motion-sickness is approaching its most severe. In the occipital IC cluster, the alpha power increase is more pronounced than the spectral increases in other frequency bands (Fig. 3-2E). In the literature, alpha activity has been regarded as the resting rhythm and has been identified as cortical idling in a way-finding experiment by Caplan *et al.* (2003). The changes in alpha power were much (~ 120 s) later than those of the subjective motion-sickness ratings, suggesting that this rhythmic activity may be related to relaxation after the long stress that is caused by the motion-sickness section.

4.3 Gender difference in motion sickness

No significant gender difference was found in motion sickness susceptibility using objective and subjective measurements in this study. This finding is consistent with those of previous study by Cheung (2003) who reported that there were no significant differences between men and women in the severity of symptoms of motion sickness while viewing an optokinetic drum (visually-induced sickness).

5 Conclusions

This study demonstrates a VR-based motion-sickness platform that comprises a 32-channel EEG and 2-channel ECG system, and a joystick with a continuous scale, where by subjects can continuously report their level of motion-sickness during experiments. All measurements, including the level of motion-sickness and the motion of the platform, were synchronized with EEG and ECG recordings. The VR-based platform simultaneously provides both visual and vestibular stimuli to generate a most realistic experimental environment for studying motion-sickness.

This study first attempted to correlate the HRV indices with the MS severity; both were recorded continuously using an ECG and a slide-type switch during a simulated driving experiment. Experiments were conducted on a motion driving simulator comprising a VR-based tunnel driving environment and a real vehicle mounted on a 6 degree-of-freedom motion platform (Lin *et al.*, 2005a; 2005b). The temporal correlation between changes in the MS severity and the HRV indices was assessed and modeled by non-linear regressive algorithms — adaptive neural fuzzy inference system (ANFIS). Some subjects who had autonomic responses opposite to those of the majority of subjects during MS exposure. These subjects (n=6 among a total of 29

subjects) likely failed to respond to VR stimulation. These subjects reported that they felt sickness immediately after the onset of the experiment. Such early onset sickness could be induced by the unfamiliar with the VR-scene. The subjects were further excluded from EEG data analysis.

The recorded EEG signals are analyzed using independent component analysis (ICA), time-frequency analysis, and time-series cross-correlation to investigate MS-related brain dynamics in a continuous driving task. Independent EEG activities and their equivalent dipole source locations were isolated by independent component analysis (ICA) to obtain the involved brain circuits during motion-sickness. The ICA signals were then correlated to the MS level to investigate the changes before, during and after motion-sickness induce session. The temporal relationship between the reported sickness-level and the involved brain circuits were then determined by cross-correlation analysis.

By combining independent component analysis, time-frequency analysis and cross correlation analysis, this work evaluates changes in the EEG power spectrum that accompanies the fluctuations in the level of motion sickness in a realistic driving task. ICA separates the multi-channel EEG signals into independent brain processes, each of which represents electrical neurophysiological activities from a tight cluster of neurons. Components with similar scalp tomography, dipole location and baseline

power spectrum from multiple subjects were grouped into component clusters. The sorting and correlation of power spectra with subjective MS levels reveal a monotonic relationship between minute-scale changes in MS and the EEG spectra of distinct component clusters (brain processes) in different frequency bands. In summary, this (1) utilized both visual and vestibular stimuli to induce realistic motion-sickness, (2) proposed a continuous rating mechanism using which subjects can report their MS level without interrupting the experiment, and (3) evaluated reproducible spectral changes in multiple brain areas that accompany fluctuations in the severity of motion sickness.

Reference

Adamson, P.B., Smith, A.L., Abraham, W.T., Kleckner, K.J., Stadler, R.W., Shih, A., & Rhodes, M.M. (2004). Continuous autonomic assessment in patients with symptomatic heart failure prognostic value of heart rate variability measured by an implanted cardiac resynchronization device. American Heart Association, 110, 2389-2394.

Arlt, J., Jahn, H., Kellner, M., & Wiedemann, K. (2003). Modulation of sympathetic activity by corticotropin-releasing hormone and atrial natriuretic peptide. European Neuropsychopharmacology, 13, S360-S360.

Arlt, J., Jahn, H., & Wiedemann, K. (2003). Modulation of sympathetic activity by corticotropin-releasing hormone and atrial natriuretic peptide. Pharmacopsychiatry, 36, 211-212.

Arribas, F.L.P., & Pineiro, A.L. (2007). Seasickness prediction in passenger ships at the design stage. Ocean Engineering, 34, 2086-2092.

Bell, A.J., Sejnowski, T.J., 1995. An information-maximization approach to blind separation and blind deconvolution. Neural Computation 7(6), 1129-1159.

Beckers, F., Verheyden, B., Ramaekers, D., Swynghedauw, B., & Aubert, A.E. (2006). Effects of autonomic blockade on non-linear cardiovascular variability indices in arts. Clinical and Experimental Pharmacology and Physiology, 33, 431-439.

Bland, B.H., Oddie, S.D., 2001. Theta band oscillation and synchrony in the hippocampal formation and associated structures: the case for its role in sensorimotor integration. Behavior Brain Research, 127(1-2), 119-136.

Bolanos, M., Nazeran, H., & Haltiwanger, E. (2006). Comparison of heart rate variability signal features derived from electrocardiography and photoplethysmography in healthy individuals. Engineering in Medicine and Biology Society, 2006. EMBS'06. 28th Annual International Conference of the IEEE, 4289-4294.

Bos, J.E., & Bles, W. (1998). Modeling motion sickness and subjective vertical mismatch detailed for vertical motions. Brain Research Bulletin, 47, 537-542.

Camm, A.J., Malik, M., Bigger, J.T., Breithardt, G., Cerutti, S., Cohen, R.J., Coumel, P., Fallen, E.L., Kennedy, H.L., Kleiger, R.E., Lombardi, F., Malliani, A., Moss, A.J., Rottman, J.N., Schmidt, G., Schwartz, P.J., & Singer, D.H. (1996). Heart rate variability: standards of measurement, physiological interpretation,

and clinical use. European Heart Journal, 17, 354-381.

Caplan, J.B., Madsen, J.R., Schulze-Bonhage, A., Aschenbrenner-Scheibe, R., Newman E.L., Kahana, M.J., 2003. Human θ oscillations related to sensorimotor integration and spatial learning. The Journal of Neuroscience 23(11), 4726-4736.

Carter, J.B., Banister, E.W., & Blaber, A.P. (2003). Effect of endurance exercise on autonomic control of heart rate. Sports medicine, 33, 33.

Casu, M., Cappi, C., Patrone, V., Repetto, E., Giusti, M., Minuto, F., & Murialdo, G. (2005). Sympatho-vagal control of heart rate variability in patients treated with suppressive doses of L-thyroxine for thyroid cancer. European Journal of Endocrinology, 152, 819.

Chen, D.D., Xu, X.H., Wang, Z.S., & Chen, J.D.Z. (2005). Alteration of gastric myoelectrical and autonomic activities with audio stimulation in healthy humans. Scandinavian Journal of Gastroenterology, 40, 814-821.

Chen, J.L., Chiu, H.W., Tseng, Y.J., & Chu, W.C. (2006). Hyperthyroidism is characterized by both increased sympathetic and decreased vagal modulation of heart rate: evidence from spectral analysis of heart rate variability. Clinical Endocrinology, 64, 611-616.

Chen, A.C., Dworkin, S.F., Haug, J., Gehrig, J., 1989. Topographic brain measures of human pain and pain responsivity. Pain 37(2), 129-141.

Cheung, B., Vaitkus, P., 1998. Perspectives of electrogastrography and motion-sickness. Brain Research Bulletin 47(5), 421-431.

Cheung, B. (2003). Lack of gender difference in motion sickness induced by vestibular Coriolis cross-coupling. Journal of Vestibular Research, 12, 191-200.

Cole, C.R., Blackstone, E.H., Pashkow, F.J., Snader, C.E., & Lauer, M.S. (1999). Heart-rate recovery immediately after exercise as a predictor of mortality. New England Journal of Medicine, 341, 1351-1357.

Collet, C., Vernet-Maury, E., Miniconi, P., Chanel, J., & Dittmar, A. (2000). Autonomic nervous system activity associated with postural disturbances in patients with perilymphatic fistula: sympathetic or vagal origin? Brain Research Bulletin, 53, 33-43.

Cowings, P.S., Naifeh, K.H., & Toscano, W.B. (1990). The stability of individual patterns of autonomic responses to motion sickness stimulation. Aviation, Space, and Environmental Medicine, 61, 399-405.

Cowings, P.S., Suter, S., Toscano, W.B., Kamiya, J., & Naifeh, K. (1986). General autonomic components of motion sickness. Psychophysiology, 23, 542-551.

Chelen, W.E., Kabrisky, M., Rogers, S.K., 1993. Spectral analysis of the electroencephalographic response to motion-sickness. Aviation, Space, and Environmental Medicine 64(1), 24-29.

Cheron, G., Leroy, A., De Saedeleer, C., Bengoetxea, A., Lipshits, M., Cebolla, A., Servais, L., Dan, B., Berthoz, A., McIntyre, J., 2006. Effect of gravity on human spontaneous 10-Hz electroencephalographic oscillations during the arrest reaction. Brain Research 1121, 104-116.

Delorme A., Makeig S., 2004. EEGLAB: an open source toolbox for analysis of single-trial EG dynamics including independent component analysis. J. Neurosci Methods 134, 9-21.

Demaree, H.A., & Everhart, D.E. (2004). Healthy high-hostiles: reduced parasympathetic activity and decreased sympathovagal flexibility during negative emotional processing. Personality and Individual Differences, 36, 457-469.

Doweck, I., Gordon, C.R., Shlitner, A., Spitzer, O., Gonen, A., Binah, O., Melamed, Y., & Shupak, A. (1997). Alterations in R–R variability associated with experimental motion sickness. Journal of the Autonomic Nervous System, 67, 31-37.

Drummond, P.D. (2002). Motion sickness and migraine: optokinetic stimulation increases scalp tenderness, pain sensitivity in the fingers and photophobia. Cephalalgia, 22, 117-124.

Eckberg, D.L. (2003). The human respiratory gate. The Journal of Physiology, 548, 339-352

Emoto, M. (2008). Wide-field video system induced motion sickness and change in viewers' sympathovagal balance. Autonomic Neuroscience: Basic and Clinical, 144, 90-90.

Emoto, M., Sugawara, M., & Nojiri, Y. (2007). Viewing angle dependency of visually-induced motion sickness in viewing wide-field images by subjective and autonomic nervous indices. Displays, 29, 90-99.

Finley, J.C., O'Leary, M., Wester, D., MacKenzie, S., Shepard, N., Farrow, S., & Lockette, W. (2004). A genetic polymorphism of the α2-adrenergic receptor increases autonomic responses to stress. Journal of Applied Physiology, 96, 2231-2239.

Forstberg, J., Andersson, E., & Ledin, T. (1998). Influence of different conditions for tilt compensation on symptoms of motion sickness in tilting trains. Brain Research Bulletin, 47, 525-535.

Franchi, F., Lazzeri, C., Barletta, G., Ianni, L., & Mannelli, M. (2001). Centrally mediated effects of bromocriptine on cardiac sympathovagal balance.

Hypertension, 38, 123-129.

Fries, P., Neuenschwander, S., Engel, A.K., Goebel, R., & Singer, W. (2001). Rapid feature selective neuronal synchronization through correlated latency shifting. Nature Neuroscience, 4, 194-200.

Gianaros, P.J., Quigley, K.S., Muth, E.R., Levine, M.E., Vasko, R.C., & Stern, R.M. (2003). Relationship between temporal changes in cardiac parasympathetic activity and motion sickness severity. Psychophysiology, 40, 39-44.

Goichot, B., Brandenberger, G., Vinzio, S., Perrin, A.E., Geny, B., Schlienger, J.L., & Simon, C. (2004). Sympathovagal response to orthostatism in overt and in subclinical hyperthyroidism. Journal of Endocrinological Investigation, 27, 348-352.

Golding, J.F. (2006). Motion sickness susceptibility. Autonomic Neuroscience: Basic and Clinical, 129, 67-76.

Gower Jr, D.W., & Fowlkes, J. (1989). Simulator sickness in the UH-60 (black hawk) flight simulator. U. S. Army Aeromedical Research Laboratory.

Greenwood, B.N., Kennedy, S., Smith, T.P., Campeau, S., Day, H.E.W., & Fleshner, M. (2003). Voluntary freewheel running selectively modulates catecholamine content in peripheral tissue and c-fos expression in the central sympathetic circuit following exposure to uncontrollable stress in rats. Neuroscience, 120, 269-281.

Griffiths, A., Das, A., Fernandes, B., & Gaydecki, P. (2007). A portable system for acquiring and removing motion artifact from ECG signals. Journal of Physics: Conference Series, 76, 012038.

Grossman, P., Wilhelm, F.H., & Spoerle, M. (2004). Respiratory sinus arrhythmia, cardiac vagal control, and daily activity. American Journal of Physiology-Heart and Circulatory Physiology, 287, 728-734.

Hayano, J., Mukai, S., Sakakibara, M., Okada, A., Takata, K., & Fujinami, T. (1994). Effects of respiratory interval on vagal modulation of heart rate. American Journal of Physiology- Heart and Circulatory Physiology, 267, 33-40.

Hermans, E.J. (2006). Defy or Ally: Neuroendocrine regulation of human socio-emotional behavior. Unpublished doctoral dissertation, Utrecht University, Utrecht,

Holmes, S.R., & Griffin, M.J. (2001). Correlation between heart rate and the severity of motion sickness caused by optokinetic stimulation. Journal of Psychophysiology, 15, 35-42.

Hu, S.Q., Grant, W.F., Stern, R.M., & Koch, K.L. (1991). Motion sickness severity and physiological correlates during repeated exposures to a rotating optokinetic drum. Aviation, Space, and Environmental Medicine, 62, 308-314.

Hughes, J.W., & Stoney, C.M. (2000). Depressed mood is related to high-frequency heart rate variability during stressors. The American Physiological Society, 62, 796-803

Holmes, S.R., Griffin, M.J., 2001. Correlation between heart rate and the severity of motion-sickness caused by optokinetic stimulation. Journal of Psychophysiology 15(1), 35-42.

Hu, S., Grant, W.F., Stern, R.M., Koch, K.L., 1991. Motion-sickness severity and physiological correlates during repeated exposures to a rotating optokinetic drum. Aviation, Space, and Environmental Medicine 62(4), 308-314.

Hu, S., McChesney, K.A., Player, K.A., Bahl, A.M., Buchanan, J.B., Scozzafava, J. E., 1999. Systematic investigation of physiological correlates of motion-sickness induced by viewing an optokinetic rotating drum. Aviation, Space, and Environmental Medicine 70(8), 759-765.

Huang, R.S., Jung, T.P., Makeig, S. 2007. Event-related brain dynamics in continuous sustained-attention tasks. In D.D. Schmorrow, L.M. Reeves (Eds.): Augmented Cognition, HCII 2007, LNAI 4565, 65–74.

Huang, R.S., Jung, T.P., Delorme, A., Makeig, S. 2008. Tonic and phasic electro-encephalographic dynamics during continuous compensatory tracking. NeuroImage 39, 1896–1909.

Jensen, O., 2001. Information transfer between rhythmically coupled networks: reading the hippocampal phase code. Neural Computation 13, 2743-2761.

Jung, T-P, Makeig, S., Humphries, C., Lee, T-W., McKeown, M.J., Iragui, V., Sejnowski, T.J., 2000. Removing Electroencephalographic Artifacts by Blind Source Separation, Psychophysiology, 37, 163-178.

Jang, D.P., Kim, I.Y., Nam, S.W., Wiederhold, B.K., Wiederhold, M.D., & Kim, S.I. (2002). Analysis of physiological response to two virtual environments: driving and flying simulation. Cyberpsychology and Behavior, 5, 11-18.

Jang, J.S.R. (1991). Fuzzy modeling using generalized neural networks and Kalman filter algorithm. Proceedings of the Ninth National Conference. on Artificial Intelligence (AAAI-91), 762-767.

Jang, J.S.R. (1993). ANFIS: adaptive-network-based fuzzy inference system. Transactions on Systems, Man and Cybernetic of the IEEE, 23, 665-685.

Jang, J.S.R., Sun, C.T., & Mizutani, E. (1997). Neuro-fuzzy and soft computing: a computational approach to learning and machine intelligence. Prentice Hall, Upper Saddle River, New Jersey, USA.

Jauregui-Renaud, K., Yarrow, K., Oliver, R., Gresty, M.A., & Bronstein, A.M. (2000). Effects of caloric stimulation on respiratory frequency and heart rate and

blood pressure variability. Brain Research Bulletin, 53, 17-23.

Kannankeril, P.J., Le, F.K., Kadish, A.H., & Goldberger, J.J. (2004). Parasympathetic effects on heart rate recovery after exercise. Journal of Investigative Medicine, 52, 394-401.

Kato, M., Sakai, T., Yabe, K., Miyamura, M., & Soya, H. (2004). Gastric myoelectrical activity increases after moderate-intensity exercise with no meals under suppressed vagal nerve activity. The Japanese Journal of Physiology, 54, 221-228.

Kellog, R.S., Castore, C., & Coward, R. (1980). Psychophysiological effects of training in a full vision simulator. Annual Scientific Meeting of the Aerospace Medical Association.

Kennedy, R.S., Lane, N.E., Berbaum, K.S., Lilienthal, M.G., 1993. Simulator sickness questionnaire: an enhanced method for quantifying simulator sickness. International Journal of Aviation Psychology 3(3), 203-220.

Klosterhalfen, S., Ruttgers, A., Krumrey, E., Otto, B., Stockhorst, U., Riepl, R.L., Probst, T., & Enck, P. (2000). Pavlovian conditioning of taste aversion using a motion sickness paradigm. Psychosomatic Medicine, 62, 671-677.

Kollai, M., & Mizsei, G. (1990). Respiratory sinus arrhythmia is a limited measure of cardiac parasympathetic control in man. The Journal of Physiology, 424, 329-342.

Kopytko, R. (2004). The affective context in non-Cartesian pragmatics: a theoretical grounding. Journal of Pragmatics, 36, 521-548.

Kuo, T.B.J., & Chan, S.H.H. (1992). Extraction, discrimination and analysis of single-neuron signals by a personal-computer-based algorithm. Neurosignals, 1, 282–292

Kuo, T.B.J., Lin, T., Yang, C.C.H., Li, C.L., Chen, C.F., & Chou, P. (1999). Effect of aging on gender differences in neural control of heart rate. American Journal of Physiology-Heart and Circulatory Physiology, 277, 2233-2239.

Kuo, T.B.J., & Yang, C.C.H. (2002). Sexual dimorphism in the complexity of cardiac pacemaker activity. American Journal of Physiology-Heart and Circulatory Physiology, 283, 1695-1702.

Kim Y.Y., Kim, H.J., Kim, E.N., Ko, H.D., Kim, H.T., 2005. Characteristic changes in the physiological components of cybersickness. Psychophysiology 42, 616-625.

Klimesch, W., 1999. EEG alpha and theta oscillations reflect cognitive and memory performance: a review and analysis. Brain Res Brain Res Rev 29, 169-195.

Klimesch, W., Doppelmayr, M., Russegger, H., Pachinger, T., Schwaiger, J., 1998. Induced alpha band power changes in the human EEG and attention. Neurosci

Lett 244, 73-76.

Levine, M.E., Muth, E.R., Williamson, M.J., & Stern, R.M. (2004). Protein-predominant meals inhibit the development of gastric tachyarrhythmia, nausea and the symptoms of motion sickness. Alimentary Pharmacology and Therapeutics, 19, 583.

Lin, C.T., Ko, L.W., Chiou, J.C., Duann, J.R., Huang, R.S., Liang, S.F., Chiu, T.W., & Jung, T.P. (2008). Noninvasive neural prostheses using mobile and wireless EEG. Proceedings of the IEEE, 96, 1167-1183.

Lin, C.T., Wu, R.C., Jung, T.P., Liang, S.F., & Huang, T.Y. (2005). Estimating driving performance based on EEG spectrum analysis. Eurasip Journal on Applied Signal Processing, 3165-3174.

Lin, C.T., Wu, R.C., Liang, S.F., Chao, W.H., Chen, Y.J., & Jung, T.P. (2005). EEG-based drowsiness estimation for safety driving using independent component analysis. Transactions on Circuits and Systems I: Fundamental Theory and Applications of the IEEE, 52, 2726-2738.

Lin, J.J.W., Duh, H.B.L., Parker, D.E., Abi-Rached, H., & Furness, T.A. (2002). Effects of field of view on presence, enjoyment, memory, andsimulator sickness in a virtual environment. Virtual Reality of the IEEE, 164-171.

Lenneman, J.K., & Backs, R.W. (2007). Diagnosticity of cardiac modes of autonomic control elicited by simulated driving and verbal working memory dual-tasks. Lecture Notes in Computer Science, 4562, 541.

Lucini, D., Norbiato, G., Clerici, M., & Pagani, M. (2002). Hemodynamic and autonomic adjustments to real life stress conditions in humans. Hypertension, 39, 184-188.

Lo, W.T., So, R.H.Y., 2001. Cybersickness in the presence of scene rotational movements along different axes. Applied Ergonomics 32, 1-14.

Makeig, S., Jung, T.P., Bell, A.J., Ghahremani, D., Sejnowski, T.J., 1997. Blind separation of auditory event-related brain responses into independent components. Proceedings of the National Academy of Sciences of the United States of America 94, 10979-10984.

Min, B.C., Chung, S.C., Min, Y.K., Sakamoto, K., 2004. Psychophysiological evaluation ofsimulator sickness evoked by a graphic simulator. Applied Ergonomics 35, 549-556.

Montano N, Porta A, Cogliati C, Costantino G, Tobaldini E, Casali KR, Iellamo F. (2008). Heart rate variability explored in the frequency domain: A tool to investigate the link between heart and behavior. Neuroscience and Biobehavioral Reviews, 33, 71-80.

Morrow, G.R., Andrews, P.L.R., Hickok, J.T., & Stern, R. (2000). Vagal changes

following cancer chemotherapy: Implications for the development of nausea. Psychophysiol., 37, 378-384.

Morrow, G.R., Roscoe, J.A., Hickok, J.T., Andrews, P.L., & Matteson, S. (2002). Nausea and emesis: evidence for a biobehavioral perspective. Supportive Care in Cancer, 10, 96-105.

Mozziconacci, S. (2001). Emotion and attitude conveyed in speech by means of prosody. 2nd Workshop on Attitude, Personality and Emotions in User-Adapted Interaction.

Mrowka, R., Persson, P.B., Theres, H., & Patzak, A. (2000). Blunted arterial baroreflex causes pathological heart rate turbulence. American journal of physiology. Regulatory, integrative and comparative physiology, 48, 1171-1175.

Ohyama, S., Nishiike, S., Watanabe, H., Matsuoka, K., Akizuki, H., Takeda, N., & Harada, T. (2007). Autonomic responses during motion sickness induced by virtual reality. Auris Nasus Larynx, 34, 303-306.

Olufsen, M.S., Alston, A.V., Tran, H.T., Ottesen, J.T., & Novak, V. (2008). Modeling Heart Rate Regulation—Part I: Sit-to-stand Versus Head-up Tilt. Cardiovascular Engineering, 8, 73-87.

Oostenveld, R., Oostendorp, T.F., 2002. Validating the boundary element method for forward and inverse EEG computations in the presence of a hole in the skull. Human Brain Mapping 17, 179-192.

Peng, S.Y., Wu, K.C., Wang, J.J., Chuang, J.H., Peng, S.K., & Lai, Y.H. (2007). Predicting postoperative nausea and vomiting with the application of an artificial neural network. British Journal of Anaesthesia, 98, 60-65.

Redfern, M.S., Yardley, L., & Bronstein, A.M. (2001). Visual influences on balance. Journal of Anxiety Disorders, 15, 81-94.

Riecke, B.E., Schulte-Pelkum, J., Caniard, F., & Bulthoff, H.H. (2005). Towards lean and elegant self-motion simulation in virtual reality. Virtual Reality of IEEE, 131–138.

Pierpont, G.L., Stolpman, D.R., & Gornick, C.C. (2000). Heart rate recovery post-exercise as an index of parasympathetic activity. Journal of the autonomic nervous system, 80, 169-174.

Pennebaker, J.W., & Skelton, J.A. (1981). Selective monitoring of bodily sensations. Journal of Personality and Social Psychology, 41, 13-223.

Pipraiya, M.R., Tripathi, L., & Dogra, G. (2005). Effects of +Gz acceleration on indices of heart rate variability. Indian Journal of Aerospace Medicine, 49, 1.

Pumprla, J., Howorka, K., Groves, D., Chester, M., & Nolan, J. (2002). Functional assessment of heart rate variability: physiological basis and practical

applications. International Journal of cardiology, 84, 1-14.

Reinvuo, T., Hannula, M., Sorvoja, H., Alasaarela, E., & Myllyla, R. (2006). Measurement of respiratory rate with high-resolution accelerometer and EMFit pressure sensor. Sensors Applications Symposium of the IEEE, 192-195

Riva, G. (1998). Virtual environment for body image modification: virtual reality system for the treatment of body image disturbances. Computers in Human Behavior, 14, 477-490.

Roach, D., Wilson, W., Ritchie, D., & Sheldon, R. (2004). Dissection of long-range heart rate variability controlled induction of prognostic measures by activity in the laboratory. Journal of the American College of Cardiology, 43, 2271-2277.

Poyhonen, M., Syvaoja, S., Hartikainen, J., Ruokonen, E., & Takala, J. (2004). The effect of carbon dioxide, respiratory rate and tidal volume on human heart rate variability. Acta Anaesthesiologica Scandinavica, 48, 93-101.

Sang, F.D.Y.P., Billar, J.P., Golding, J.F., & Gresty, M.A. (2003). Behavioral methods of alleviating motion sickness: effectiveness of controlled breathing and a music audiotape. Journal of Travel Medicine, 10, 108-111.

Santarcangelo, E.L., Balocchi, R., Scattina, E., Manzoni, D., Bruschini, L., Ghelarducci, B., & Varanini, M. (2008). Hypnotizability-dependent modulation of the changes in heart rate control induced by upright stance. Brain research bulletin, 75, 692-697.

Schlegel, T.T., Brown, T.E., Wood, S.J., Benavides, E.W., Bondar, R.L., Stein, F., Moradshahi, P., Harm, D.L., Fritsch-Yelle, J.M., & Low, P.A. (2001). Orthostatic intolerance and motion sickness after parabolic flight. Journal of Applied Physiology, 90, 67-82.

Shanthi, C., & Kumaravel, N. (2005). Non-linear analysis of cardiac autonomic nervous activity using principal dynamic fluctuation Analysis. INDICON, 2005 Annual IEEE, 208-211.

Shores, M.M., Pascualy, M., Lewis, N.L., Flatness, D., & Veith, R.C. (2001). Short-term sertraline treatment suppresses sympathetic nervous system activity in healthy human subjects. Psychoneuroendocrinology, 26, 433-439.

Stauss, H.M. (2003). Heart rate variability. The American Physiological Society, 285, 927-931

Stys, A., & Stys, T. (1998). Current clinical evidence of heart variability. Clinical Cardiology, 21, 719–724.

Sugita, N., Yoshizawa, M., Tanaka, A., Abe, K., Chiba, S., Yambe, T., & Nitta, S. (2004). Quantitative evaluation of the effect of visually-induced motion sickness using time coherence function between blood pressure and heart rate.

Engineering in Medicine and Biology Society, 2004. 26th Annual International Conference of the IEEE, 4, 2407–2410

Thayer, J.F. (2007). What the heart says to the brain (and vice versa) and why we should Listen. Psychological Topics, 16, 241-250.

Tracey, K.J. (2007). Physiology and immunology of the cholinergic antiinflammatory pathway. Journal of Clinical Investigation, 117, 289-296.

Uijtdehaage, S.H.J., Stern, R.M., & Koch, K.L. (1993). Effects of Scopolamine on autonomic pofiles underlying motion sickness susceptibility. Aviation, Space, and Environmental Medicine, 64, 1-8.

Von-Borell, E., Langbein, J., Despres, G., Hansen, S., Leterrier, C., Marchant-Forde, J., Marchant-Forde, R., Minero, M., Mohr, E., & Prunier, A. (2007). Heart rate variability as a measure of autonomic regulation of cardiac activity for assessing stress and welfare in farm animals—A review. Physiology & Behavior, 92, 293-316.

Wood, M.J., Struve, F.A., Straumanis, J.J., Stewart, J.J., Wood, C.D., 1991. The effect of motion-sickness on brain waves (EEG). Aviation, Space, and Environmental Medicine 62, 461.

Wood, C.D., Stewart, J.J., Wood, M.J., Struve, F.A., Straumanis, J.J., Mims, M.E., Patrick, G.Y., 1994. Habituation and motion-sickness. Journal of Clinical Pharmacology 34, 628-634.

Wood, S.J., 2002. Human otolith-ocular reflexes during off-vertical axis rotation: effect of frequency on tilt-translation ambiguity and motion-sickness. Neuroscience Letters 323(1), 41-44.

Wu, J.P., 1992. EEG changes in man during motion-sickness induced by parallel swing. Space Medicine and Medical Engineering 5(3), 200-205.

Wan, H., Hu, S., & Wang, J. (2003). Correlation of phasic and tonic skin-conductance responses with severity of motion sickness induced by viewing an optokinetic rotating drum. Perceptual and motor Skills, 97, 1051-1057.

Wodey, E., Senhadji, L., Pladys, P., Carre, F., & Ecoffey, C. (2003). The relationship between expired concentration of sevoflurane and sympathovagal tone in children. Anesthesia and Analgesia, 97, 377-382.

Xu, L.H., Koch, K.L., Summy-Long, J., Stern, R.M., Seaton, J.F., Harrison, T.S., Demers, L.M., & Bingaman, S. (1993). Hypothalamic and gastric myoelectrical responses during vection-induced nausea in healthy Chinese subjects. American Journal of Physiology- Endocrinology and Metabolism, 265, 578-584.

Yang, C.C.H., Chao, T.C., Kuo, T.B.J., Yin, C.S., & Chen, H.I. (2000). Preeclamptic pregnancy is associated with increased sympathetic and decreased

parasympathetic control of HR. American Journal of Physiology-Heart and Circulatory Physiology, 278, 1269-1273.

Yardley, L., & Redfern, M.S. (2001). Psychological factors influencing recovery from balance disorders. Journal of Anxiety Disorders, 15, 107-119.

Yerdelen, D., Acil, T., Goksel, B., & Karatas, M. (2008). Heart rate recovery in migraine and tension-type headache. Headache, 48, 221.

Yokota, Y., Aoki, M., Mizuta, K., Ito, Y., & Isu, N. (2005). Motion sickness susceptibility associated with visually induced postural instability and cardiac autonomic responses in healthy subjects. Acta Otolaryngologica, 125, 280-285.

Young, L.R. (2003). Adaptation of the vestibulo-ocular reflex, subjective tilt, and motion sickness to head movements during short-radius centrifugation. Journal of Vestibular Research, 13, 65-77.

Zhong, Y., Jan, K.M., Ju, K.H., & Chon, K.H. (2006). Quantifying cardiac sympathetic and parasympathetic nervous activities using principal dynamic modes analysis of heart rate variability. American Journal of Physiology-Heart and Circulatory Physiology, 291, 1475.

Ziavra, N.V., Sang, F., Golding, J.F., Bronstein, A.M., & Gresty, M.A. (2003). Effect of breathing supplemental oxygen on motion sickness in healthy Adults. Mayo clinic proceedings, 78, 574-579.